

DESY 96-049

ISSN 0418-9833

DTP/96/20

March 1996

Working Group Report on the STRUCTURE OF THE PROTON ‡

B. Badelek

Institute of Experimental Physics, Warsaw University, PL-00681, Warsaw, Poland,
and Physics Institute, University of Uppsala, S-751 21 Uppsala, Sweden

J. Bartels

II Institut für Theoretische Physik, Universität Hamburg, D-22761 Hamburg,
Germany

N. Brook

Department of Physics, University of Glasgow, Glasgow, G12 8QQ, Scotland

A. De Roeck

DESY, Notkestrasse 85, D-22603 Hamburg, Germany

T. Gehrmann

Department of Physics, University of Durham, Durham, DH1 3LE, England

M. Lancaster

Department of Physics, University of Oxford, Oxford, OX1 3NP, England

A. D. Martin

Department of Physics, University of Durham, Durham, DH1 3LE, England

A. Vogt

DESY, Notkestrasse 85, D-22603 Hamburg, Germany

On leave from Sektion Physik, Universität München, D-80333 Munich, Germany

Abstract. We summarize the developments on the structure of the proton that were studied at the Workshop on “HERA Physics” that was held in Durham in September 1995. We survey the latest structure function data; we overview the QCD interpretations of the measurements of the structure functions and of final state processes; we discuss charm production and the spin properties of the proton.

‡ To be published in the Proc. of the Durham Workshop on “HERA Physics: Proton, Photon and Pomeron Structure”, J. Phys. G.

1. Introduction

One of the highlights of the previous Durham Workshop on HERA physics in March 1993 was the presentation [1], for the first time, of the measurements of the proton structure function $F_2(x, Q^2)$, which showed a dramatic rise with decreasing x . They immediately ruled out a Regge-based description, which is so successful for hadronic and photoproduction ($Q^2 = 0$) cross sections. The Regge model predicts a much slower rise with decreasing x than was observed in deep inelastic measurements of F_2 . The observation generated great activity at the 1993 Workshop, particularly as application of the BFKL equation [2] had anticipated a singular $x^{-\lambda}$ growth with decreasing x . To quote from the Introduction to the Proceedings [3]:

“The argument over the interpretation of the rise began immediately and continued all week — was it evidence for the singular BFKL behaviour of the gluon; was it just evidence of the need for a different input parametrization; what did it imply for the Pomeron and diffractive scattering? Although the protagonists tried very hard, it will take a lot more data and quite a few more Workshops to answer all these exciting questions!”

Now two and a half years on, at the time of this Workshop (September 1995), the measurements by H1 and ZEUS have indeed improved remarkably. Our knowledge of diffractive scattering has blossomed and it now has its own Working Group. Both the precision and the kinematic range of the HERA measurements of F_2 have greatly increased. We now have measurements for $x < 10^{-4}$ and $Q^2 \sim 1.5 \text{ GeV}^2$. In fact one of the tasks undertaken at the Workshop was a study of the consistency between all the measurements of F_2 (see section 2). The present surprise is that the strong rise of F_2 with decreasing x appears to persist down to the lowest observed Q^2 ($Q^2 \sim 1.5 \text{ GeV}^2$) and yet the photoproduction measurements show that the slow rise of the conventional Regge description works well at $Q^2 = 0$. The transition from the “soft” to the “hard” regime appears to be very rapid. It is appropriate to review our knowledge of the low Q^2 behaviour of F_2 ; section 3 contains a summary of our discussions. In fact sections 2 and 3 contain an overview of all deep inelastic data. The high precision measurements of the fixed-target experiments are now being extended, for $F_2(ep)$ at least, to much lower x by the experiments at HERA. Specially compiled plots are presented to demonstrate the complementary nature of these experiments, as well as to indicate their relative errors. Also we summarize the information obtained about nuclear shadowing.

Partons satisfying the conventional GLAP(Altarelli-Parisi) [4] evolution seem to be well able to describe the new HERA and fixed-target deep inelastic data down to as low as $Q^2 \sim 1 \text{ GeV}^2$. Could this be an indication of the precocious onset of perturbative QCD and the absence of higher twists? Such a conclusion would be premature. At larger x ($x \gtrsim 0.01$) there are many different types of high-precision fixed-target constraints on the individual parton distributions and, with the possible exception of the gluon, the partons are well determined. On the other hand at small x ($x \lesssim 10^{-3}$) we have, so far, only one type of structure function measurement, namely $F_2(x, Q^2)$, and there are many different partonic descriptions at small x , particularly as we have to supply the (non-perturbative) partonic input at some scale Q_0^2 for the GLAP leading $\log Q^2$ limit, or at some x_0 for the BFKL leading $\log(1/x)$ limit, of the perturbative QCD evolution. At small x the dominant parton is the gluon and the description of the observables is driven by the behaviour of the gluon distribution.

According to perturbative QCD we expect the small x behaviour of the (sea) quark and gluon distributions to be strongly correlated due to the $g \rightarrow q\bar{q}$ transition. In section 4 we overview the different QCD contributions to F_2 at small x . We see that F_2 is too inclusive a measurement to be easily able to distinguish the dominant underlying perturbative QCD component at small x . Thus some of the questions of 1993 remain, but we now have a much clearer idea why the search for the answers is so difficult.

Unlike the conventional GLAP gluon distribution, the BFKL distribution $f(x, k_T^2)$ is unintegrated over the transverse momentum k_T of the gluon. The BFKL gluon has two main characteristics. It has the familiar $x^{-\lambda}$ growth with decreasing x , but accompanied by a diffusion in k_T — typically a Gaussian distribution in $\log k_T^2$ about some initial transverse momentum which broadens as $\sqrt{\log(1/x)}$ as x decreases. The inclusive measurement F_2 integrates over this characteristic k_T^2 dependence and, worse, they sample contributions arising from diffusion to the (non-perturbative) low k_T region (see section 4). This suggests the value of studying deep inelastic final state processes which simultaneously expose both the characteristic x and k_T^2 dependence of the BFKL gluon. Section 5 discusses two such measurements, the energy flow in the central region and the production of forward jets. Whereas the former one seems to be very sensitive to (unknown) hadronization effects and therefore, in its present form, cannot be considered to be a reliable test for BFKL dynamics, the second approach looks more promising: data of the 1993 HERA run are confronted with both the analytical BFKL prediction and fixed-order matrix element calculations, and the agreement with the BFKL calculation is quite encouraging.

We devote section 6 to charm production at HERA, processes which are directly driven by the gluon. Both open charm, for instance the sizeable charm component F_2^c of F_2 , and J/ψ production processes offer valuable information on the small x behaviour of the gluon distribution. We discuss the status of fixed-order calculations of F_2^c , present numerical predictions and try to answer in some detail to what extent the measurement of the charm component of F_2 can be used to pin down the gluon structure function. Particular attention is also given to J/ψ production which may be able to discriminate between different gluon distributions.

Last, but not least, in section 7 we summarize our discussions on the spin structure of the proton. Many experiments, prompted by the original surprising result on the proton spin structure function by EMC, are now yielding much information. After a brief introduction of the general background we give an overview of the present experimental situation and the status of the Bjorken and Ellis-Jaffe sum rules. The small x behaviour of g_1 seems to be of particular interest: evaluation of the first moment Γ_1 requires an appreciable extrapolation of g_1 , while recent QCD predictions indicate a rather strong rise of g_1 in the small x region. Finally section 8 contains some brief conclusions.

2. Overview of structure function data

2.1. Introduction

Here we review the status of the data on structure functions and derived quantities. Until a few years ago this knowledge came entirely from fixed-target experiments. Now it is being complemented and extended by the results from the HERA ep collider, especially in the region of low x where the dynamics of a large number of confined partons has to be understood, as well as at very high scales where the perturbative assumptions can be further tested.

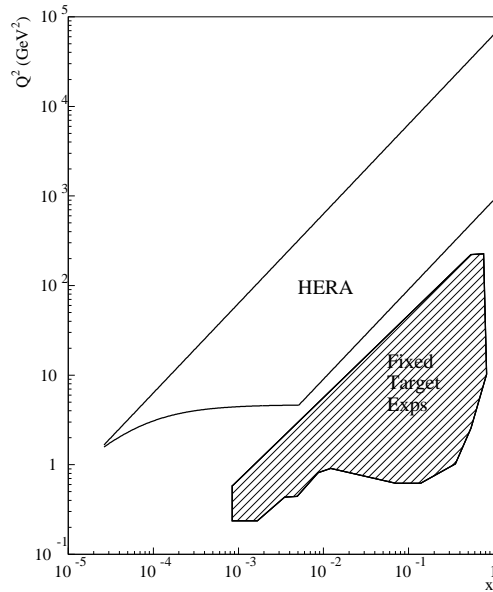


Figure 2.1. The kinematical region covered by the HERA and fixed-target experiments.

At this Workshop the HERA experiments presented results from the 1994 data taking period [5]. During this period HERA collided 27.5 GeV positrons on 820 GeV protons, as opposed to the 26.7 GeV electrons in 1992 and 1993. The centre-of-mass energy of the ep collision is 300 GeV. The new F_2 results extend to larger Q^2 values due to a tenfold increase in statistics, compared to the data collected in 1993 (and about a factor of hundred increase with respect to the 1992 data, on which the results shown at the previous Durham workshop were based). Furthermore both the H1 and ZEUS experiments have made a special effort to obtain measurements at lower values of Q^2 so as to explore the region towards $Q^2 \rightarrow 0$. Values of Q^2 down to about 1 GeV² have been reached as a result of detector upgrades, operating HERA in a different collision mode called shifted interaction vertex mode, and by using events with initial state QED radiation from the incoming lepton. At the time of the Workshop all data were still preliminary, but by now have become final to a large extent [6, 7]. For the QCD interpretation of the data, such as the extraction of the gluon density, the 1993 data

will be used.

In the HERA experiments, the scattered electron as well as the hadronic final state are measured. Apart from tantalizing questions on the dynamics of the hadronic final state itself (see Section 5) this allows us to determine the kinematics both from the scattered electron and from the hadronic final state. In practice, for the latter, a mixture of the hadron and electron information is used, rather than exclusively hadronic final state quantities.

The kinematic plane covered by HERA and the fixed-target measurements is shown in Fig. 2.1. Generally measurements at HERA can reach $Q^2(x)$ values two orders of magnitude larger (smaller) than those reached by fixed-target experiments. Fig. 2.1 shows that the two regions make contact and thus the continuity and normalization of the data can be checked. New upgrades of the HERA detectors will allow the exploration of even lower Q^2 in the future.

The (unpolarised) fixed-target deep-inelastic scattering programme will come to an end in 1996 except for the continuation of the CCFR neutrino experiments. Many experiments (SLAC, BCDMS, EMC, NMC, E665, CDHSW, BEBC and CCFR) have contributed to the heroic and successful effort to obtain a fundamental and precise knowledge of properties of partons and of QCD. Characteristics of a number of them are listed in Table 2.1. The fixed-target electron (muon) scattering experiments were almost always inclusive, i.e. information on the kinematic variables came only from measurements of the incident and scattered leptons. In the charged-current neutrino experiments the outgoing muon and the total energy of the produced hadrons are measured, and in neutral-current experiments only the latter is detected.

In deep-inelastic experiments the low x region is correlated with low values of Q^2 , as shown in Fig. 2.1. For fixed-targets the lowest values of x were reached by the NMC at CERN and E665 Collaboration at FNAL applying special experimental techniques permitting measurements of muon scattering angles as low as 1 mrad. These “small x triggers” and special off-line selection methods were also effective against the background of muons scattered elastically from target atomic electrons which produce a peak at $x = 0.000545$. Systematic errors on F_2 in both experiments (in particular those on the ratio of structure functions for different nuclei, F_2^a/F_2^b) were greatly reduced as a result of exposing several target materials at the time and/or by a frequent exchange of targets in the beam.

Table 2.1. Fixed-target experiments contributing to the F_2 measurements. The x and Q^2 ranges refer to the F_2 data; structure function ratio measurements extend the low limits by approximately an order of magnitude.

Beam	Targets	Experiment	$Q^2(\text{GeV}^2)$	x
e	p,d,A	SLAC	0.6 – 30	0.07 – 0.8
μ	p,d,A	BCDMS	7.5 – 230	0.07 – 0.6
μ	p,d,A	NMC	0.5 – 75	0.006 – 0.6
μ	p,d,A	E665	0.2 – 75	0.0008 – 0.6
$\nu, \bar{\nu}$	Fe	CCFR, CDHSW	1.0 – 500	0.015 – 0.6

In the one-photon-exchange approximation, the differential electroproduction cross section is related to the structure function $F_2(x, Q^2)$ and the ratio $R(x, Q^2)$ of the cross

sections for the longitudinally and transversally polarised virtual photons by

$$\frac{d^2\sigma(x, Q^2)}{dQ^2 dx} = \frac{4\pi\alpha^2}{Q^4 x} \left[1 - y - \frac{Mxy}{2E} + \left(1 - \frac{2m^2}{Q^2} \right) \frac{y^2(1 + 4M^2x^2/Q^2)}{2(1 + R)} \right] F_2(x, Q^2) \quad (2.1)$$

where M and m are the mass of the proton and the electron respectively, and E is the incident lepton energy. For the HERA kinematics by neglecting M and m this expression reduces to:

$$\frac{d^2\sigma}{dx dQ^2} = \frac{4\pi\alpha^2}{Q^4 x} \left[1 - y + \frac{y^2}{2(1 + R)} \right] F_2(x, Q^2). \quad (2.2)$$

The function $R(x, Q^2)$ has so far been measured only in fixed-target experiments, but even here information is scarce. The usual procedure to determine the $F_2(x, Q^2)$ is to assume a value of $R(x, Q^2)$ (theoretical, experimental or a combination of these) and then to extract $F_2(x, Q^2)$ from the data, using an iterative comparison of the experimental yield (corrected for acceptance, inefficiency of the apparatus as well as for higher-order QED processes) with the electroproduction cross section. For the HERA measurements R was calculated using the QCD relation [8] with the GRV structure function parametrization. At small x and Q^2 the assumed R values can be as large as 1. Note that a 20% error on R corresponds to about a 2% uncertainty on F_2 at $y = 0.6$ for R of about 0.6. The effects due to Z boson exchange for neutral current interactions in the presently covered high Q^2 region for F_2 at HERA regime amount to a few percent only. New data on $R(x, Q^2)$ from fixed-target experiments will be discussed in Section 2.5.

In this Section we present the status of the F_2 measurements at HERA and in the fixed-target experiments, QCD fits to these data, measurements of $R(x, Q^2)$ and tests of the (flavour singlet and nonsinglet) sum rules.

2.2. Measurement of $F_2(x, Q^2)$ at HERA

Both the H1 and ZEUS experiments have released new data on structure function measurements at small x . It was noted above, that to determine the kinematical variables x and Q^2 , we can use two out of four experimentally accessible quantities: the energy, E'_e , and angle, θ_e , of the scattered electron, and the energy, E_h , and average angle, θ_h , of the hadron flow. The ultimate method is a global fit of all observed quantities, which requires a level of understanding of the detector response and of the error correlations that the experiments have not yet achieved. In total four methods are currently used in the analyses to reconstruct the event kinematics. The electron method, is the method used so far in all fixed-target experiments. Here the basic formulae for Q^2 and y are

$$y_e = 1 - \frac{E'_e}{E_e} \sin^2 \frac{\theta_e}{2} \quad Q_e^2 = 4E'_e E_e \cos^2 \frac{\theta_e}{2} = \frac{E_e'^2 \sin^2 \theta_e}{1 - y_e}. \quad (2.3)$$

The polar angle θ_e is defined with respect to the proton beam direction, referred to as ‘‘forward’’ region. E_e is the incident electron energy. It remains at HERA the most precise way to reconstruct Q^2 in the whole kinematic range. However at low y ($y < 0.1$) the measurement of x becomes poor and at large y ($y > 0.8$) the radiative corrections which need to be applied to the observed cross section to extract the Born

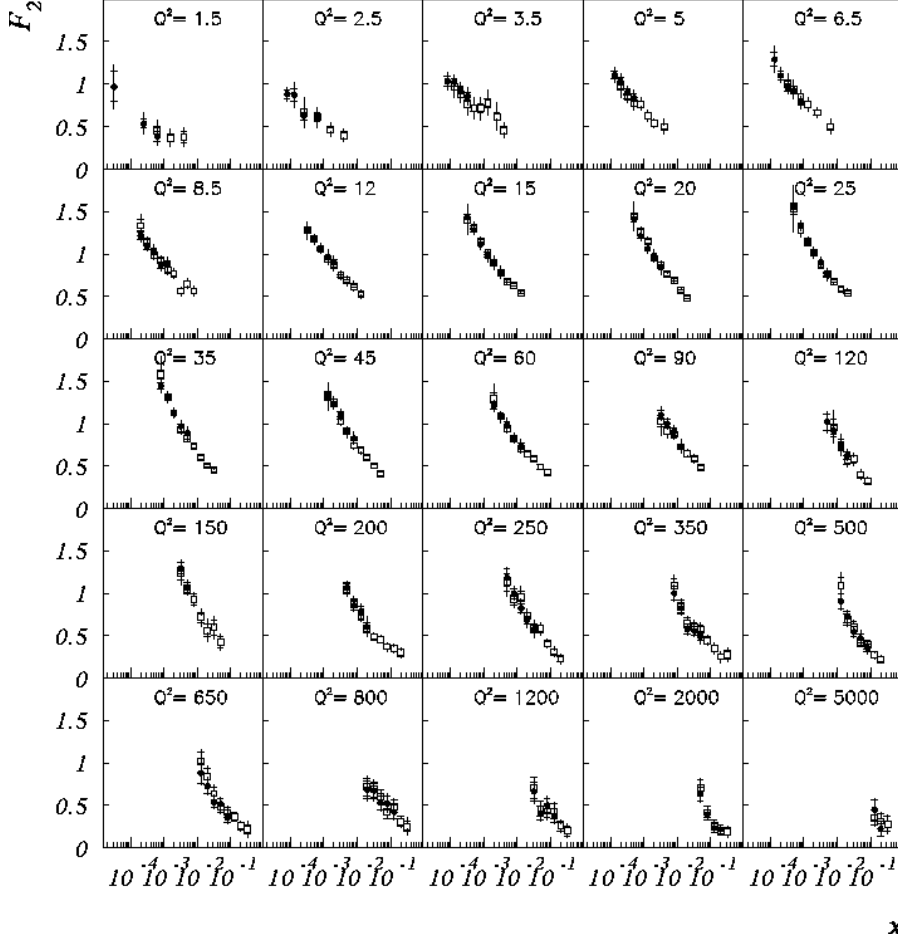


Figure 2.2. Measurement of the structure function with the electron (closed circles) and the Σ method (open squares) by the H1 Collaboration. The inner error bar is the statistical error. The full error bar represents the statistical and systematic errors added in quadrature disregarding the luminosity error (1.5%).

cross section are very large. The mixed method used by the H1 Collaboration in 1992 takes Q^2 from the electron and y from the hadronic variables (y_h) according to

$$y_h = \frac{\sum_h (E - P_z)_h}{2E_e} \quad (2.4)$$

where the sum includes all detected hadrons h , which have an energy E and longitudinal momentum component P_z . The resolution of y_h is better than the resolution of y_e for low y values but becomes inferior at large y values. For the double angle method (DA) [11] only the angles of the scattered electron and the hadronic system are used. The method is almost independent of energy scales in

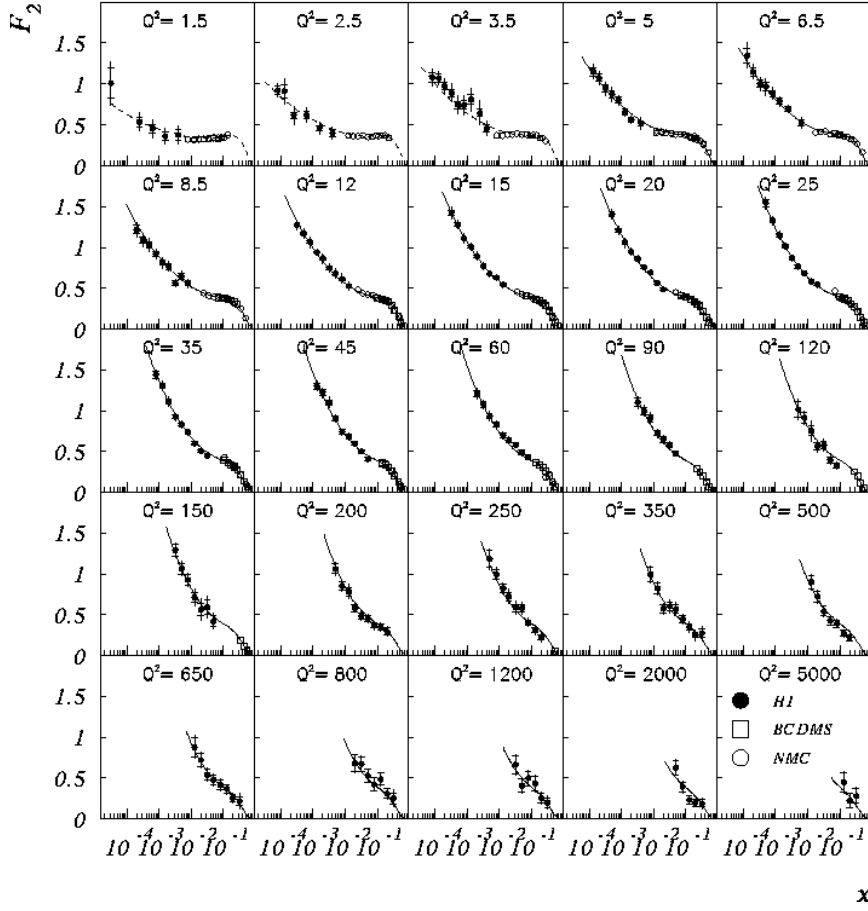


Figure 2.3. Measurement of the structure function $F_2(x, Q^2)$ as function of x . The closed circles are H1 data, the open circles are data from NMC [9] and BCDMS [10]. The inner error bar is the statistical error. The full error bar represents the statistical and systematic errors added in quadrature disregarding the luminosity errors. The curves represent the NLO QCD fit, discussed in Section 2.4.

the calorimeters but, at very low y , the method is very sensitive to noise in the calorimeters. The variables y and Q^2 are reconstructed from

$$y_{DA} = \frac{\sin \theta_e (1 - \cos \theta_h)}{\sin \theta_h + \sin \theta_e - \sin(\theta_e + \theta_h)} \quad Q_{DA}^2 = 4E_e^2 \frac{\sin \theta_h (1 + \cos \theta_e)}{\sin \theta_h + \sin \theta_e - \sin(\theta_e + \theta_h)} \quad (2.5)$$

with

$$\tan \frac{\theta_h}{2} = \frac{\Sigma_h(E - P_z)_h}{P_{T,h}^2}. \quad (2.6)$$

This method has been used by the ZEUS Collaboration. A new method used by the H1 Collaboration [12, 13], called the Σ method (Σ), determines y and Q^2 from

$$y_{\Sigma} = \frac{\sum_h (E - P_z)_h}{(E - P_z)_e + \sum_h (E - P_z)_h} \quad Q_{\Sigma}^2 = \frac{E_e'^2 \sin^2 \theta_e}{1 - y_{\Sigma}} \quad (2.7)$$

where the sum runs over all hadrons in the numerator and over all hadrons plus the scattered electron in the denominator. In this method the energy of the incident electron in the interaction is reconstructed, which reduces drastically the sensitivity to the main radiative process. The resolution in x at low y is good enough to allow the H1 Collaboration to reach $y = 0.01$. The resolution at large y is worse but less sensitive to radiative corrections than when using only the measurement of the scattered electron. For precision measurements of the structure function the different methods are used to control the systematics of event smearing and radiative corrections. In Fig. 2.2 the results using the electron and Σ methods are compared for the H1 data, showing a very good agreement.

Due to the inevitable beampipe hole for detectors at a collider, the scattered electron has to have a minimum angle to leave the beampipe and be detected. From (2.3) it follows that this leads to a minimum requirement on Q^2 , which is also visible in Fig. 2.1. To study whether F_2 still rises at lower values of Q^2 , several ways to increase the acceptance for low Q^2 were explored.

The ZEUS detector was improved for electron detection around the beampipe by the addition of a scintillator strip detector on the face of the rear calorimeter. This allowed the detection of the scattered electron down to smaller angles (175.5° compared to 174° in 1993) with a large improvement of the angular resolution (2 mrad compared to 7 mrad in 1993). The detector was also used to make an event-by-event correction to the scattered electron energy arising from the energy loss in the inactive material prior to the calorimeter, thereby improving the energy resolution and reducing the energy scale uncertainty. Due to the large statistics the electron energy scale and angular shift uncertainty for the the H1 results have been reduced to 1% and 1 mrad respectively. H1 could also – due to the excellent accelerator conditions at the end of the 1994 running period – make use of the most inner active elements of the calorimeter, and increase its low scattering angle acceptance from 173° to 174° . In 1993 H1 initiated a pilot project to shift the interaction vertex of the collisions towards the forward (proton) region. They demonstrated that collisions produced at a position shifted by about 70 cm downstream of the detector could still be used for F_2 analysis, and allowed an increase in the acceptance from 8.5 GeV^2 to 4.5 GeV^2 for the 1993 data. In 1994 about 10 times more data were accumulated using this method, and results have been shown by both experiments.

Another way to access low Q^2 is by using a sample of deep inelastic events with an energetic photon (e.g. $E_{\gamma} > 4 \text{ GeV}$) emitted collinear with the incident electron. These radiative events can be interpreted as deep inelastic scattering events with a reduced incident energy $E_r = E_e - E_{\gamma}$ which can be reconstructed through the detection of the radiated photon in the small angle photon tagger of the luminosity system of the experiments. When using the electron method, the “true” kinematic variables y_t and Q_t^2 for such an ep collision are obtained by replacing in (2.3) the nominal beam energy by the reduced energy E_r . Both experiments have shown data using this process [6, 7].

In summary, compared to the previous analyses, the F_2 measurement has been extended to lower and higher Q^2 (from $4.5 - 1600 \text{ GeV}^2$ to $1.5 - 5000 \text{ GeV}^2$), and to lower and higher x (from $1.8 \times 10^{-4} - 0.13$ to $3 \times 10^{-5} - 0.32$). The final result is

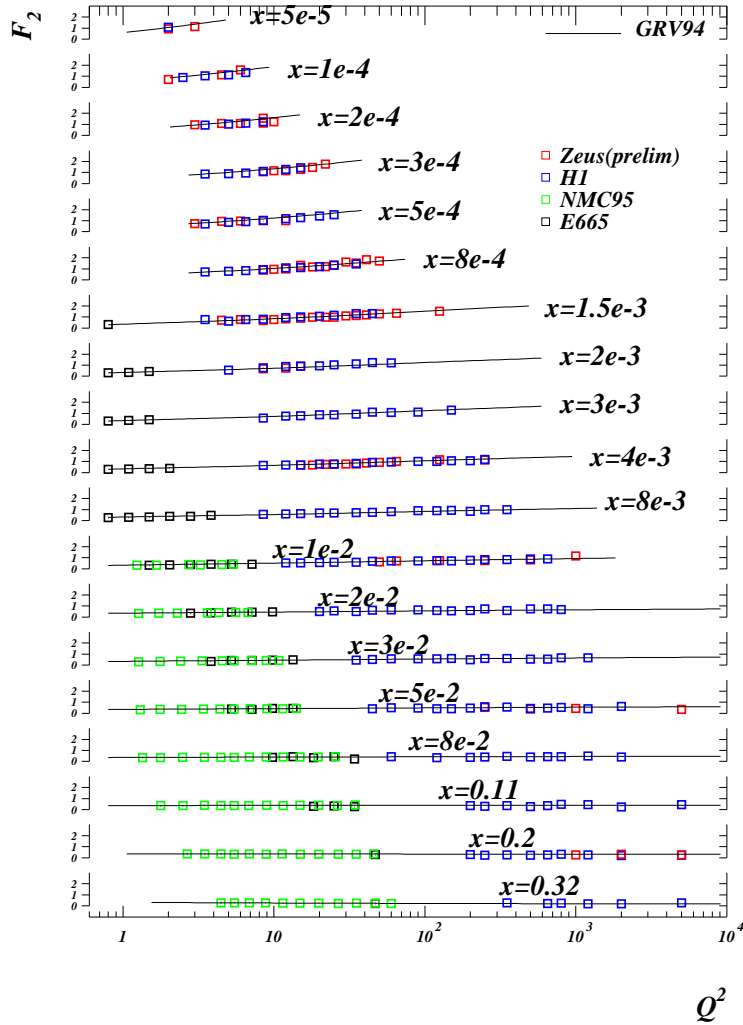


Figure 2.4. Measurement of the structure function $F_2(x, Q^2)$ as function of Q^2 for the H1, ZEUS, NMC and E665 experiments. The curve is the prediction of the GRV parton distributions.

shown in Fig. 2.3 as a function of x and in Fig. 2.4 as a function of Q^2 . The error bars of the data are now reduced to the 5% to 10% level (except at high and very low Q^2). The normalization uncertainty has been reduced to 1.5% (2.5%) for H1 (ZEUS). The rise of F_2 with decreasing x is confirmed with higher precision. This rise continues, albeit less strongly than at higher Q^2 , in the region of the lowest Q^2 available. Scaling violations are clearly seen in the plot of F_2 versus Q^2 and will be interpreted in terms of QCD below.

To emphasize the rise of F_2 at low Q^2 , data from the eight lowest Q^2 bins are shown and compared with recent F_2 parametrizations in Fig. 2.5. It demonstrates that the rise of F_2 towards low x is also present in the low Q^2 region. The measurement is in good agreement with recent data from fixed-target experiments E665 and NMC at

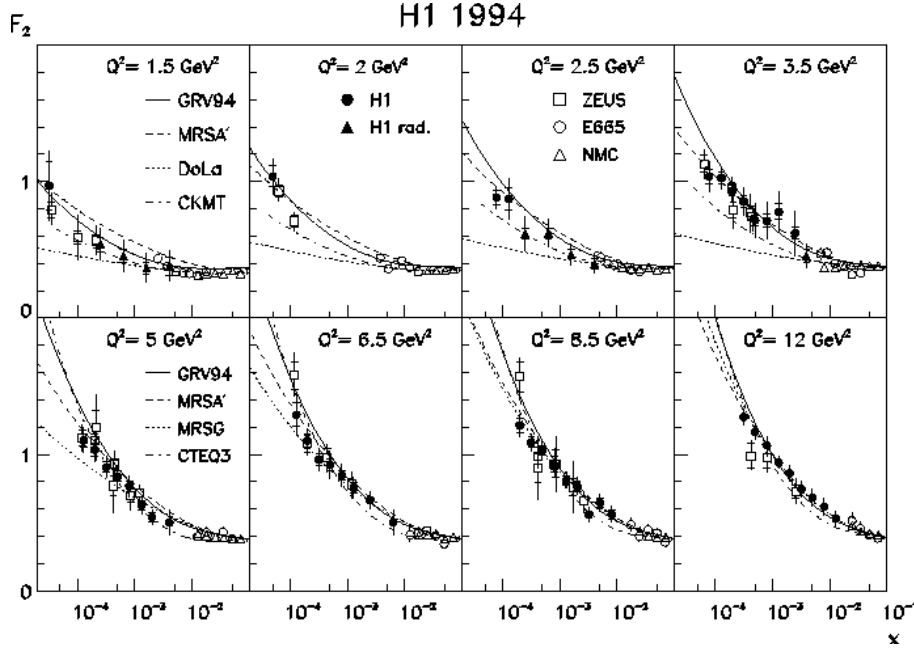


Figure 2.5. Measurement of the proton structure function $F_2(x, Q^2)$ in the low Q^2 region by H1 (closed circles: non-radiative events; closed triangles: radiative events), together with results from the ZEUS (open squares), E665 (open points) and NMC (open triangles) experiments. Different parametrizations for F_2 are compared to the data. The DOLA and CKMT curves are only shown for the upper row of Q^2 bins; CTEQ3M and MRS3 are shown for the lower row; GRV and MRSA' are shown for the full Q^2 range. The Q^2 values of the ZEUS data shown for the bins $Q^2 = 3.5, 5$ and 6.5 GeV^2 are measurements at $3.0, 4.5$ and 6 GeV^2 respectively.

higher x values. The curves represent GLAP QCD inspired predictions (GRV [14], MRS [15] and CTEQ [16]) and two Regge inspired predictions (DOLA [17] and CKMT [18]). The Regge inspired predictions, shown only for the lowest Q^2 bins, are generally below the data.

The persistent rise of F_2 at low x for small Q^2 indicates that the photoproduction regime has not been reached yet. This can also be seen in Fig. 2.6 which shows for the low Q^2 data the strong rise of F_2 as a function of W , the invariant mass of the γ^*p system (at low x , $W \simeq \sqrt{Q^2/x}$). F_2 is related to the total cross section of the proton-virtual photon interaction $\sigma_{tot}(\gamma^*p)$ via

$$\sigma_{tot}(\gamma^*p) \simeq \frac{4\pi^2\alpha}{Q^2} F_2(W, Q^2). \quad (2.8)$$

The F_2 growth can be contrasted with the weak rise with W of the total real photoproduction cross section in the same range of W , as shown in Fig. 2.6. The different behaviour for $Q^2 = 0$ and data at a finite small Q^2 remains one of the interesting questions to be studied at HERA.

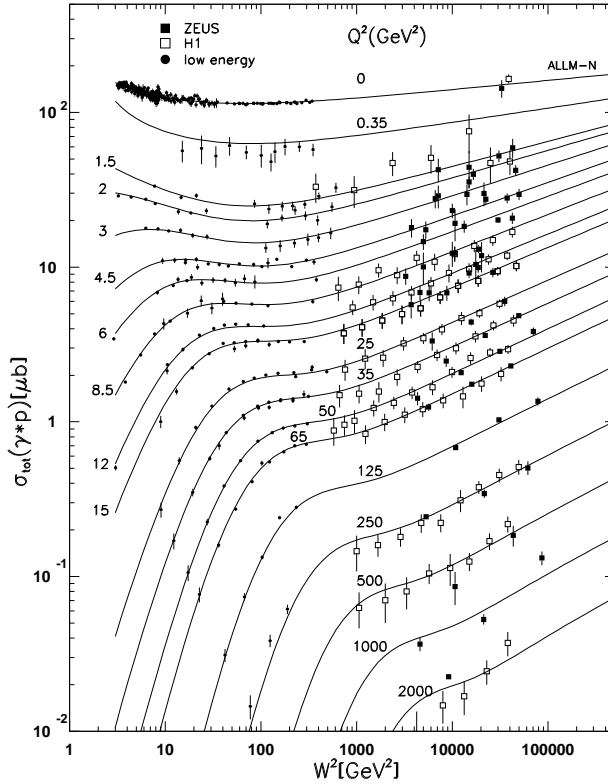


Figure 2.6. Measurement of the proton structure function $F_2(W, Q^2)$ as function of W^2 . The inner error bar is the statistical error. The full error represents the statistical and systematic errors added in quadrature. Also data at $Q^2 = 0$ are shown. Note that this figure contains the preliminary H1 data [19]. The curves are an ALLM parametrization [20].

2.3. Fixed-target structure function data

The NMC has presented their analysis of the proton and deuteron structure functions [9], in the range $0.006 \leq x \leq 0.6$ and $0.5 \leq Q^2 \leq 75 \text{ GeV}^2$, as shown for F_2^d in Fig. 2.7, performed on the almost final sample of events. A clear scaling violation pattern with slopes $d \ln F_2 / d \ln Q^2$ positive at low x and an “approach to scaling” (i.e. a rise of F_2 from $Q^2 = 0$ to the scaling region) is visible. In this figure a comparison of the NMC, SLAC [21] and BCDMS [10] measurements is also shown. All three data sets are in good agreement with each other. They were thus used to obtain parametrizations of F_2^p and F_2^d and their uncertainties, using a 15-parameter function. The low x results of the EMC NA2 experiment have earlier been disproved by the NMC measurements. The data confirm a characteristic weak x dependence of F_2 at low Q^2 , observed for the first time by the EMC NA28 experiment [22] and also interpreted in [23] (see also Section 3).

New measurements of the proton and deuteron structure functions for $x > 0.0001$ have recently been presented by the E665 Collaboration and are shown in Fig. 2.8 [24]. The lowest Q^2 and x values in their data are 0.2 GeV^2 , and 8×10^{-4} respectively. A clear pattern emerges from these data at Q^2 values lower than a few GeV^2 , namely a weak x , and possibly a stronger than logarithmic Q^2 dependence, of F_2 .

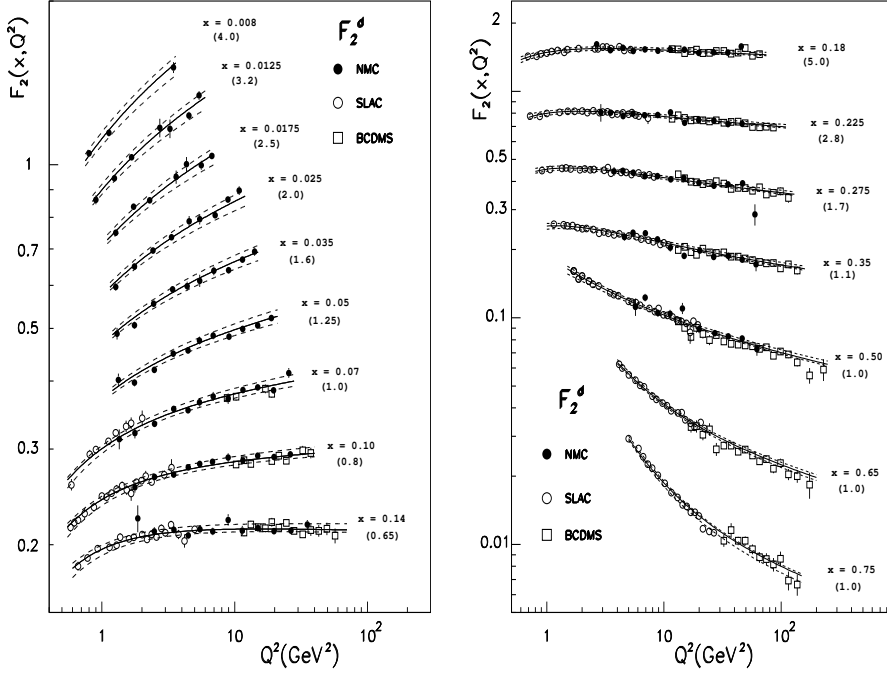


Figure 2.7. The data from NMC compared with the data from SLAC and BCDMS. The errors are statistical. The solid curves are the results of a 15-parameter fit to all three data sets. The dashed curves correspond to the extreme values of the parameters (from [9]).

The E665 region of x , i.e. $x > 10^{-5}$, is now being investigated by both the H1 and ZEUS Collaborations at HERA. The most dramatic effect visible in the HERA large Q^2 data is a strong increase of F_2 with decreasing x , while there is a rather weak x dependence of the F_2 observed by EMC NA28, NMC, and E665.

The fixed-target F_2 data have had great impact on the determination of parton distributions (see e.g. [25]). It is now seen that these data join well to the results of HERA and thus make a joint QCD analysis possible in a large kinematic interval (see below). In Fig. 2.9 a detailed comparison of the structure function F_2 as function of Q^2 between H1, ZEUS, E665 and NMC is shown for x values around 0.2, 0.07, 0.05 and 0.012. The data show a smooth continuation over the whole Q^2 region. It also shows a (still) substantially different level of accuracy between the HERA and the fixed-target experiments. The former are still expected to improve both in statistics and systematics in the next few years. Apart from the above overall agreement, there exists however a discrepancy between the NMC and CCFR F_2 data at low x (not shown). This was much discussed at the Workshop, but did not result in any new conclusion.

Both the NMC and E665 experiments have measured the deuteron to proton structure function ratio, F_2^d/F_2^p , extending down to very low values of x . In the case of NMC the ratio has been measured directly, i.e. the measurement of the absolute structure function is used only for calculation of the radiative corrections. The data are usually presented as the ratio F_2^n/F_2^p where F_2^n is defined as $2F_2^d - F_2^p$. This quantity would give the structure function of the free nucleon in the absence of nuclear effects in

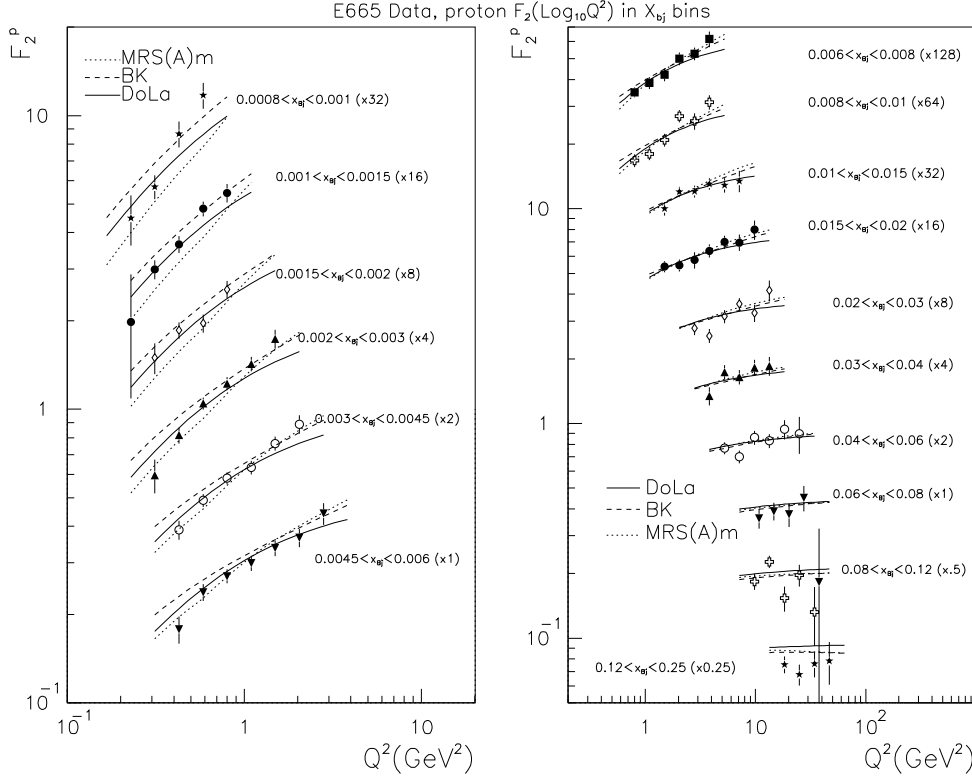


Figure 2.8. Measurements of F_2^p by the E665 Collaboration. The errors are statistical and systematic added in quadrature, a normalisation uncertainty (1.8%) is not included. Curves show model calculations of Martin, Stirling and Roberts, Badelek and Kwiciński, and Donnachie and Landshoff (from [24]).

the deuteron. The results are presented on the left in Fig. 2.10 [26]. In both data sets the average Q^2 varies from bin to bin reaching down to $\langle Q^2 \rangle = 0.2 \text{ GeV}^2$ at $x = 0.0008$ for the NMC and $\langle Q^2 \rangle = 0.004 \text{ GeV}^2$ at $x = 5 \times 10^{-6}$ for E665. The results of both experiments show that the ratio F_2^n/F_2^p remains below unity down to the smallest measured values of x . At low x this can be attributed to nuclear shadowing in the deuteron [27], predicted to be only weakly x dependent, as observed. It seems unlikely that the results can also indicate a difference in F_2 of protons and neutrons at low x , since e.g. in Regge models the difference between the proton and neutron structure functions vanishes with decreasing x [27, 28, 29].

New data have appeared on nuclear shadowing. NMC have performed a high precision study of the A dependence of nuclear shadowing in the range $0.004 < x < 0.6$ and $1.5 \text{ GeV}^2 < Q^2 < 60 \text{ GeV}^2$. The results are shown on the right in Fig. 2.10 [30]. These measurements of the ratios F_2^A/F_2^C for $A = \text{Be, Al, Ca, Fe, Sn and Pb}$ taken in conjunction with those on D, He, Li, C and Ca [31, 32] and with earlier data of SLAC [33], show a detailed pattern of the x dependence of shadowing. The NMC data range from $A = 2$ to $A = 208$. The functional dependence of F_2^A/F_2^C on A has been parametrized as $F_2^A/F_2^C = cA^{(\alpha-1)}$ in each bin of x . The amount of shadowing increases strongly with the mass number A . Lower values of x and Q^2 are covered by the nuclear data of E665 in the region $x > 0.0001$ and $Q^2 > 0.1 \text{ GeV}^2$ [34], as shown in

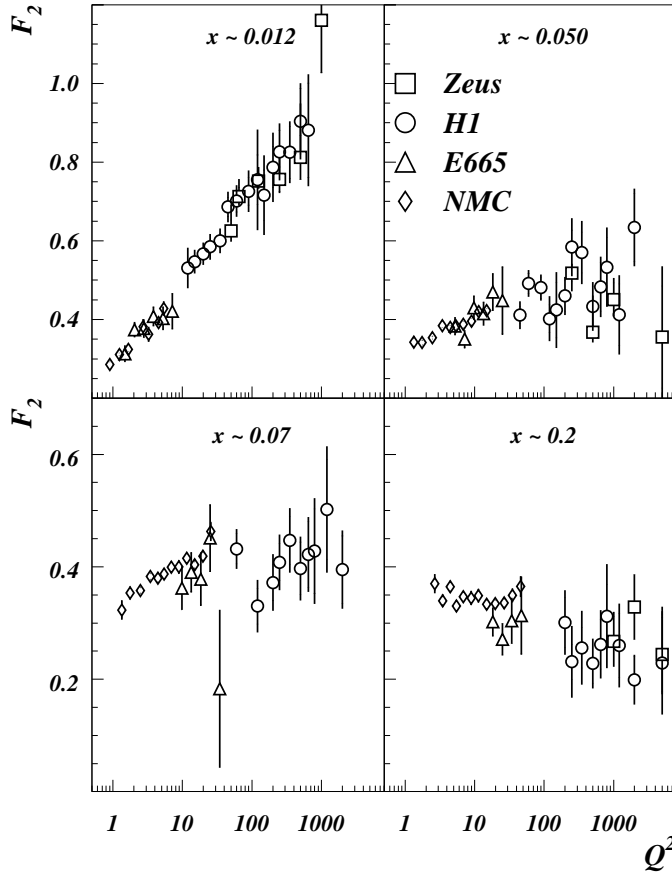


Figure 2.9. Detailed comparison of the structure function F_2 as function of Q^2 between H1, ZEUS, E665 and NMC, for x values around 0.2, 0.07, 0.05 and 0.012. The error bars represent the full errors on the data points.

Fig. 2.11 (left). A decrease in the amount of shadowing observed by E665 is presently under discussion. Shadowing seems to saturate at x about 0.004 as also indicated by the NMC data on the F_2^{Li}/F_2^D and F_2^C/F_2^D ratios measured down to $x=0.0001$ and $Q^2=0.03$ GeV² [32]. No clear Q^2 dependence is visible in the E665 data in a wide interval of Q^2 , shown in Fig. 2.11 (right), contrary to the preliminary NMC results in which positive Q^2 slopes for the F_2^{Sn}/F_2^C ratio at $x < 0.1$ are observed, as shown in [35]. The shadowing region seems to have another interesting feature: it contains a large fraction of large rapidity gap (or diffractive) events, their fraction increasing with A [36].

2.4. Parton distribution measurements

Both the H1 and ZEUS experiments have performed next-to-leading order (NLO) QCD fits based on the Altarelli–Parisi (GLAP) evolution equations on the HERA and fixed-target F_2 data. Fig. 2.3 shows that the F_2 data can be well described by such a QCD fit. Note that only data with $Q^2 \geq 5$ GeV² were used in the fit. The fit result was evolved to lower Q^2 and used as a prediction in the region $Q^2 < 5$ GeV². The low

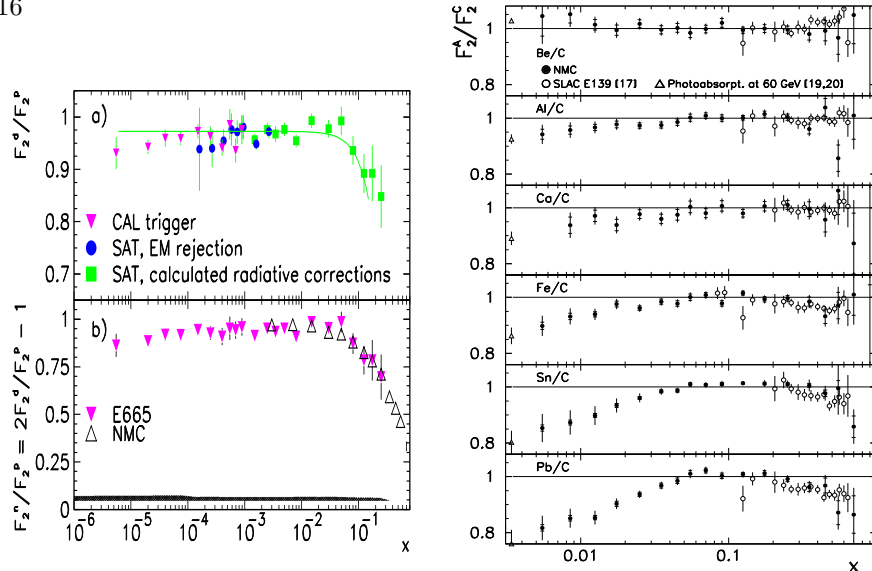


Figure 2.10. Left: E665 results. a) F_2^d/F_2^p for three different techniques of extracting the ratio. The curve shows a prediction of Badelek and Kwiciński, [27]. b) $2F_2^n/F_2^p = 2F_2^d/F_2^p - 1$ as a function of x . The NMC data at $Q^2 = 4 \text{ GeV}^2$ are also shown. Errors are statistical. The systematic uncertainty is represented by the hatched area in Fig. b) (from [26]). Right: NMC results on F_2^A/F_2^C , averaged over Q^2 (open symbols) together with earlier results of SLAC (closed symbols). Inner/outer error bars represent the statistical/total errors. The SLAC-E139 data for silver and gold were used for the comparison with the tin and lead data of the NMC, respectively. The photoproduction cross section data are given at a small value of x for convenience (from [30]).

Q^2 data are found to be well described. This result suggests that, within the present accuracy, no (large) higher twist terms are required in this region, contrary to the NMC fit, see below. This may need to be reviewed when higher precision data at low x become available.

The scaling violations from the HERA data allow an estimate of the gluon density $xg(x)$ at low values of x , while the fixed-target data are needed to constrain the high x region. The H1 QCD fit [37] includes only proton data from H1, NMC and BCDMS. Additionally the momentum fraction carried by the gluon is imposed to be 0.44. Apart from the ZEUS data, the ZEUS fit [38] includes data from NMC, both on proton and deuteron targets. The results are shown in Fig. 2.12 for $Q^2 = 20 \text{ GeV}^2$. The error bands shown include a careful analysis of the systematics, taking into account the correlation between different sources. The results of the two experiments agree very well. The resulting gluon distribution shows a clear rise with decreasing x . Similar results have been found in [15], which include also other data than those from structure functions. In the region $x > 10^{-2}$ the extracted gluon densities agree with the result obtained by the NMC.

NLO QCD fits have been performed by the NMC to their (earlier) accurate measurements of the structure functions F_2^p and F_2^d down to low values of x [39]. The flavour singlet and non-singlet quark distributions as well as the gluon distribution have been parametrized at the reference scale equal to 7 GeV^2 . All the data with $Q^2 \geq 1 \text{ GeV}^2$ were included in the fit. Besides the leading twist contribution a higher twist term was also included using a factor $1 + H(x)/Q^2$ where $H(x)$ was determined from the SLAC and the BCDMS measurements [40], averaged over the proton and

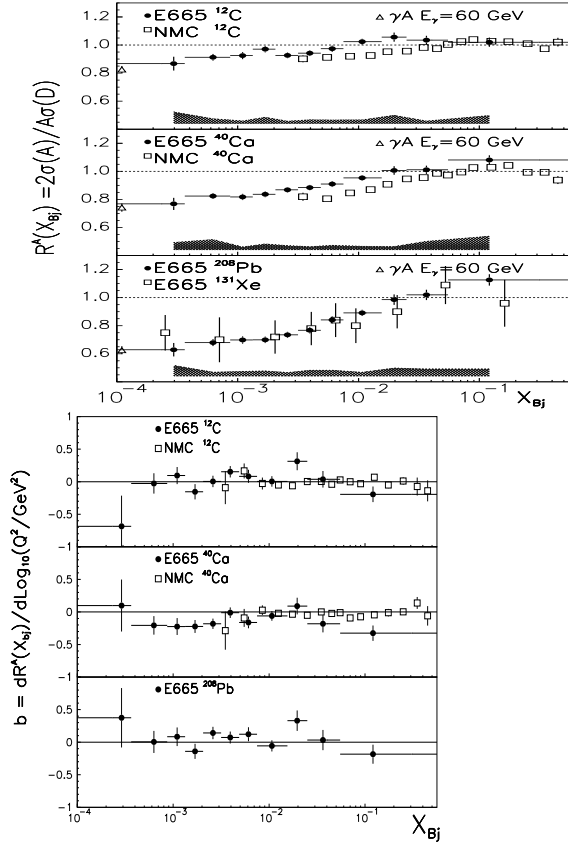


Figure 2.11. Left: E665 results on σ^A/σ^D . Errors are statistical, the systematic ones are marked as shaded bands. Overall normalisation uncertainties have not been included. The NMC results have been shown for comparison where available (from [34]). Right: Q^2 dependence of the E665 F_2^A/F_2^D data (closed circles). Errors result from the fit, in which only statistical errors were considered. The NMC results are drawn as open squares (from [34]).

deuteron, and suitably extrapolated to lower values of x . Results of the QCD fit to the proton structure function data are shown in Fig 2.13 and clearly indicate the extension of the QCD analysis to the low x and low Q^2 regions. The contribution of higher twists is however substantial at scales of about 1 GeV^2 .

Additional information on the gluon density is extracted from hadronic final states. The H1 experiment has extracted the gluon density from 2-jet events. The method and results are given in [41, 42]. The results are limited to the region $x \geq 0.001$, and agree with the gluon extracted from scaling violations. The E665 experiment has used the energy–energy angular pattern of hadrons produced in DIS to extract the gluon distribution function of the nucleon, down to $x=0.005$.

An interesting point in the QCD analysis arises from the presence of diffractive-like events in the deep inelastic scattering event sample. A contribution of approximately 10% from events with a large rapidity gap towards the proton remnant, and with the characteristics as measured in hadronic diffractive exchange, has been established [43].

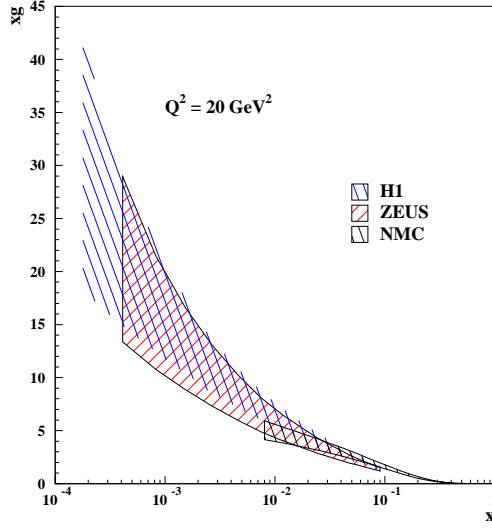


Figure 2.12. The gluon density $xg(x)$ at 20 GeV^2 extracted from a NLO QCD fits by the H1 [37], ZEUS [38] and NMC [39] Collaborations.

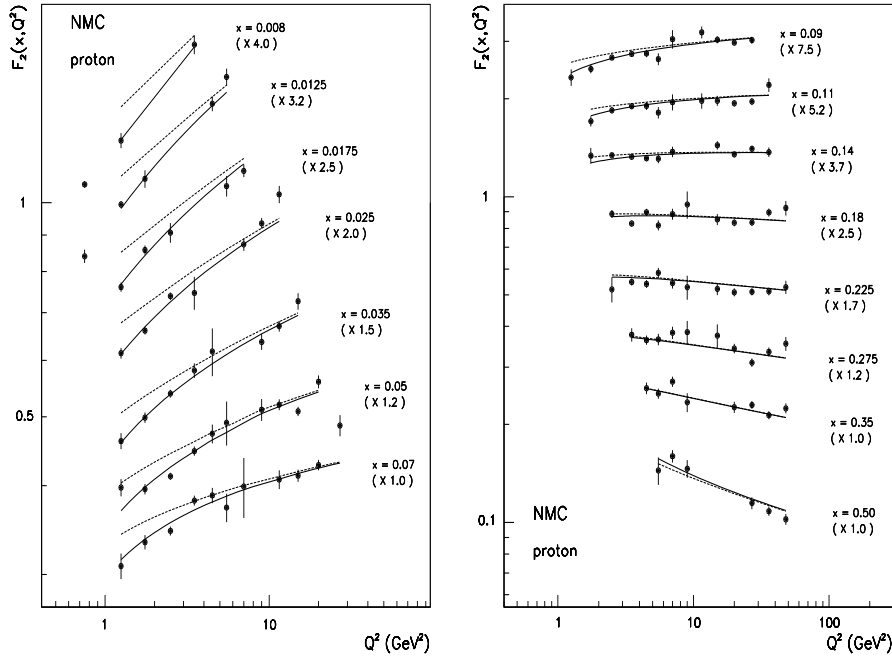


Figure 2.13. The results of the QCD fit to the F_2^p data. The solid line is the result of the QCD fit with higher twist included. The dotted curve shows the contribution of F_2^{LT} . The errors are statistical (from [39]).

These events possibly originate from a different production mechanism than the one for the bulk of the deep inelastic data. So far no special account has been taken of this in the extraction of partons from inclusive F_2 measurements; this topic was discussed at the Workshop and should be considered further.

2.5. $R(x, Q^2)$ measurements

Extraction of $F_2(x, Q^2)$ from the data needs information on $R(x, Q^2)$. In particular the ratio of inelastic cross sections on different nuclei is only equal to the corresponding structure function ratio, provided $R(x, Q^2)$ is the same for these nuclei. Results of the NMC analysis on $R^{Ca} - R^C$ [45] and $R^d - R^p$ [46], shown in Fig 2.14 (left), demonstrate that neither of these quantities exhibit a significant dependence on x and that they are both compatible with zero. The NMC reported preliminary measurements of $R(x, Q^2)$ for proton and deuteron targets as a function of x in the range $0.006 < x < 0.14$ [47]. The average Q^2 of these measurements ranges from 1.1 GeV^2 at the smallest x to 15.5 GeV^2 at $x=0.14$. The results show a rise of R with decreasing (small) x . Preliminary measurements of $R(x, Q^2)$ on a heavy target (Fe), at $x > 0.01$ and $Q^2 > 4 \text{ GeV}^2$ (at present) have also been reported by the CCFR neutrino Collaboration [48]. In their data analyses the NMC and E665 experiments assumed R was independent of the target atomic mass A and given by the SLAC parametrization [49] valid for $x > 0.1$ and $Q^2 > 0.3 \text{ GeV}^2$. This parametrization was then extrapolated (with 100% error) to $Q^2 \rightarrow 0$. Hence there is a need of a theoretical estimate of R (or F_L) in the region of low x and low Q^2 . Two ongoing phenomenological studies are expected to deliver such estimates soon. In these studies both the perturbative QCD contribution, which at low x and low Q^2 is dominated by the photon-gluon mechanism, and a non-perturbative term are taken into account. In [50] the latter contribution is determined phenomenologically (Fig. 2.14 (right)) while in [48] it is fitted to the low Q^2 data.

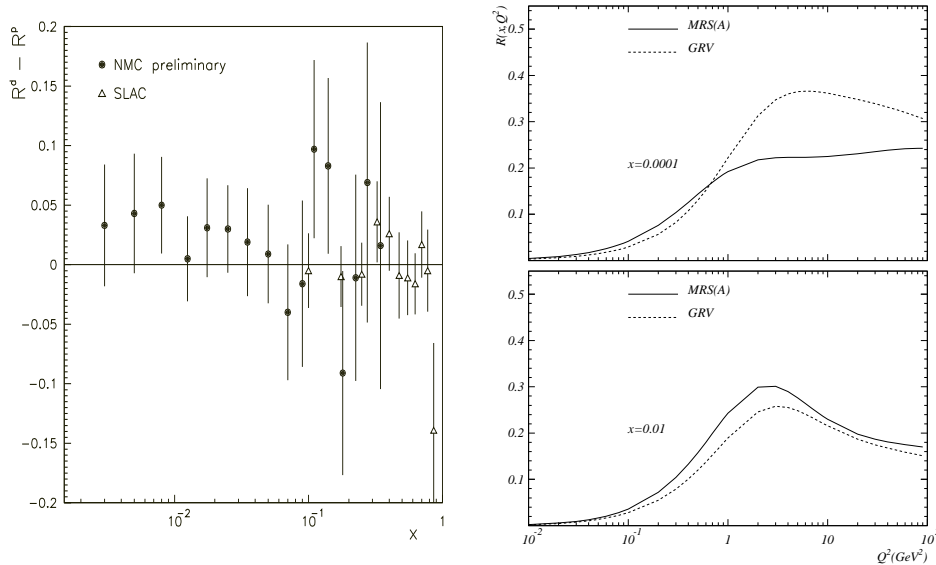


Figure 2.14. Left: NMC (preliminary) results $R^d - R^p$ compared with the QCD predictions (the curve) and with the results of SLAC (open symbols), from [46]. Right: $R(x, Q^2)$ in the phenomenological model of Badelek, Kwiciński and Staśto, for two different parton parametrisations (from [50]).

Also at HERA the study of R is an issue of interest. For this purpose it has been proposed to operate HERA at lower energies, to have the cross section measurements at two y values for a given x, Q^2 point. Such a measurement could be done in 1996 or

1997. A discussion on this topic is presented in [5].

2.6. Sum Rules

Several sum rules have been formulated for different combinations of structure functions. Strict QCD predictions, valid for $Q^2 \rightarrow \infty$, exist for those involving only flavour nonsinglet contributions: the Gross–Llewellyn-Smith and the Bjorken sum rules. Experimental measurements of such sum rules provide a stringent test of fundamental QCD assumptions. They also in principle permit the extraction of the strong coupling constant, α_S , from the data. Due to the finite Q^2 of the measurements, a predicted value of a sum rule is usually presented in the form of a power series in α_S , the coefficients of which are directly calculated.

There is no strict QCD prediction for the sum rules containing the flavour singlet contributions, i.e. the Gottfried and Ellis–Jaffe sum rules. The reason is that singlet contributions contain an “intrinsic” Q^2 dependence. Testing them usually results in surprises which teach us a lot about the shortcomings of the simple quark model.

All the sum rules involve integrations over the whole $0 \leq x \leq 1$ interval. This means that due to the limited experimental acceptance, interpolations from x_{min} to 0 and from x_{max} to 1 have to be performed. Usually the former is more problematic due to a larger contribution of the small x region to integrals and/or to a poor theoretical understanding of this kinematic region. Thus the extrapolation $x \rightarrow 0$ is a major source of systematic errors in such sum rule tests. Another source is produced by the limited experimental acceptance in Q^2 at each x value. This usually means that a sum rule is measured at a certain Q_0^2 , common to all points but at values of Q_0^2 which are not sufficiently high to exclude a contribution from nonperturbative effects (“higher twists”).

2.6.1. Tests of the flavour nonsinglet sum rules. The Bjorken sum rule involves the spin structure functions and will be presented in Section 7. The Gross-Llewellyn-Smith sum rule, formulated within the Quark Parton Model, states that the integral over the valence quark densities is equal to 3 i.e. $\int_0^1 xF_3(x)dx/x=3$. The QCD corrections to this rule have been calculated up to α_S^3 [51]. The sum rule has been tested by the CCFR Collaboration in conjunction with additional low energy data from bubble chamber experiments [52]. The sum rule is fulfilled at the 10% accuracy level. The value of α_S has been obtained at $Q^2=3$ GeV²; it corresponds to $\alpha_S(M_Z) = 0.108_{-0.005}^{+0.003}(\text{stat.}) \pm 0.004(\text{syst.})_{-0.006}^{+0.004}(\text{HT})$. The uncertainty due to the low scale of the measurement (i.e. the presence of “higher twists”) dominates the statistical error.

2.6.2. Tests of the flavour singlet sum rules. The NMC measurements of F_2^d (fitted together with the SLAC and BCDMS data) and of F_2^n/F_2^p allow a determination of the Gottfried sum i.e. $S_G = \int (F_2^p - F_2^n)dx/x$ where $F_2^p - F_2^n = 2F_2^d(1 - F_2^n/F_2^p)/(1 + F_2^n/F_2^p)$. At $Q^2 = 4$ GeV², neglecting any Q^2 dependence, S_G was found to be 0.235 ± 0.026 [53], significantly below the simple quark-parton model value of $1/3$. This is evidence for a flavour asymmetric sea in the nucleon (\bar{d} sea quarks carry more momentum than \bar{u}), a fact confirmed by the NA51 measurement of the Drell-Yan asymmetry in pp and pn collisions, which gave: $\bar{u}/\bar{d}=0.51 \pm 0.04 \pm 0.05$ at $x=0.18$ and $Q^2=25$ GeV² [54]. Recently a non-negligible Q^2 dependence of $F_2^p - F_2^n$ as a function of x at low Q^2 has been reported by the NMC: both the position of the maximum and the maximum value of this function change with Q^2 . This change

becomes negligible when higher twist contributions are separated out from the F_2^d and F_2^n/F_2^p measurements [55]. The Ellis–Jaffe sum rule, involving the spin structure functions will be discussed in Section 7.

3. Low Q^2 , low x insights from fixed-target data

3.1. Introduction and basic concepts

Due to the experimental constraints the fixed-target studies of deep inelastic scattering at low x necessarily were correlated with low Q^2 ($Q^2 \lesssim 1 \text{ GeV}^2$). There are two reasons why this kinematic region is of special interest. First, as emphasized in section 2, the new HERA measurements at small x highlight the importance of a theoretical understanding of the connection between the low Q^2 and high Q^2 behaviour. The second is a practical reason; a unified treatment of low and high Q^2 is essential for the large Q^2 data analysis, since to implement radiative corrections we require a knowledge of structure functions for $Q_{meas}^2 \geq Q^2 \geq 0$.

At low Q^2 there are constraints on the structure functions $F_i(x, Q^2)$ which follow from eliminating the kinematical singularities at $Q^2 = 0$ from the hadronic tensor $W^{\mu\nu}$. It is easy to show that as $Q^2 \rightarrow 0$ we require

$$F_2 = O(Q^2) \quad \text{and} \quad F_L = O(Q^4). \quad (3.1)$$

Hence it is clear that Bjorken scaling, which holds approximately at high Q^2 , cannot be a valid concept at low Q^2 .

In dealing with low Q^2 data we need to introduce the concept of “higher twists”. The operator product expansion leads to the representation

$$F_2(x, Q^2) = \sum_{n=0}^{\infty} \frac{C_n(x, Q^2)}{(Q^2)^n} \quad (3.2)$$

where the functions $C_n(x, Q^2)$ depend weakly (i.e. logarithmically) on Q^2 . The various terms in this expansion are referred to as leading ($n = 0$) and higher ($n \geq 1$) twists. The QCD improved parton model where

$$F_2(x, Q^2) = x \sum_i e_i^2 [q_i(x, Q^2) + \bar{q}_i(x, Q^2)] + O(\alpha_S(Q^2)), \quad (3.3)$$

and which gives approximate Bjorken scaling, retains only the leading twist contribution. Physically the higher twist effects arise from the struck parton’s interaction with target remnants, thus reflecting confinement. For Q^2 of the order of a few GeV^2 , contributions of the “higher twists” may become significant, see, for example, ref. [39]. Contrary to the common opinion higher twists, which are corrections to the leading (approximately scaling) term (3.3), can only be implemented for sufficiently large Q^2 . Thus they cannot correctly describe the low Q^2 (i.e. nonperturbative) region since the expansion (3.2) gives a divergent series there. In particular the individual terms in this expansion violate the constraint (3.1). In order to correctly describe this region the (formal) expansion (3.2) has to be summed beforehand, at large Q^2 , and then analytically continued to the region of $Q^2 \sim 0$. This is automatically embodied in certain models like the Vector Meson Dominance (VMD) model. To be precise the VMD model together with its generalisation which gives (approximate) scaling at large Q^2 can be represented in a form (3.2) for sufficiently large Q^2 .

In practical applications to the analysis of experimental data which extend to the moderate values of Q^2 one often includes the higher twists corrections in the following simplified way:

$$F_2(x, Q^2) = F_2^{LT}(x, Q^2) \left[1 + \frac{H(x)}{Q^2} \right] \quad (3.4)$$

where the F_2^{LT} is the leading twist contribution to F_2 and $H(x)$ is determined from fit to the data. This simple minded expression may not be justified theoretically since in principle the higher twist terms, i.e. functions $C_n(x, Q^2)$ for $n \geq 1$ in eq.(3.2) evolve differently with Q^2 than the leading twist term.

Here we give a brief overview of the parametrizations and the data in the low x , low Q^2 region. We refer the reader to refs. [56] and [57] for a more detailed review of the treatment of low Q^2 problems.

3.2. Parametrisations of structure functions

There exist several phenomenological parametrizations (fits) of the structure function F_2 which incorporate the $Q^2 \rightarrow 0$ constraints as well as the Bjorken scaling behaviour at large Q^2 [58, 59, 17, 60, 61, 18]. Certain parametrizations [60, 61, 18] also contain the (QCD motivated) scaling violations. However, they usually are not linked with the conventional QCD evolution. Nor is the low Q^2 behaviour related to the explicit vector meson dominance, known to dominate at low Q^2 . There exist parametrizations which explicitly contain QCD evolution: [14, 23, 62, 63]. Most of the parametrizations essentially extend the parton model formula for F_2 down to the low Q^2 region modifying in a suitable way the parton distributions; the model [23] includes also the VMD contribution besides the partonic one and is an absolute prediction (i.e. no fitting to the data). The low Q^2 modifications are typically the following ones:

- (i) Instead of the variable x , modified variables $\bar{x}_i = x(1 + Q_{0i}^2/Q^2)$ are used as arguments of the parton distributions where ‘ i ’ enumerates the type of the parton.
- (ii) Models which at large Q^2 include the QCD scaling violations, have the evolution in Q^2 either “frozen” below certain scale Q_0^2 which is of the order of 1 GeV² or the evolution in a “shifted” variable $Q^2 + Q_0^2$ is used.
- (iii) Parton distribution functions are multiplied by form factors of the type $Q^2/(Q^2 + m_i^2)$ which ensure vanishing of the structure function $F_2(x, Q^2)$ at $Q^2 = 0$.

Modifications are absent in the dynamical model [14] which, in principle, is meant to describe the structure functions only in the large Q^2 region even if the QCD evolution is extended down to very low scales. Also the recent parametrization of the “parton distributions” [63] uses the variable x instead of \bar{x} . This model does not however extend down to the very low values of Q^2 (i.e. for $Q^2 < 0.25$ GeV²) and, in particular, it does not accommodate the photoproduction.

Parametrizations of $F_2(x, Q^2)$ differ in their small x behaviour. Most of them (except [61] and [17]) incorporate at large Q^2 the steep rise of $F_2(x, Q^2)$ as the function of x with decreasing x which is much stronger than implied (for instance) by the expectations based on the “soft” pomeron with intercept $\alpha_P = 1.08$. This steep increase of $F_2(x, Q^2)$ becomes very weak at low Q^2 . Possible dynamical origin of this

effect is different in different models being either attributed to the absorptive effects [18, 62, 63], to the onset of the VMD mechanism [23] or to the pure perturbative QCD effects related to the change of the “evolution length” [14].

There exists practically only one parametrisation of the $R(x, Q^2)$ structure function for the nucleon, i.e. the SLAC parametrisation, [49], based on measurements by SLAC, EMC, BCDMS and CDHSW and valid at $x > 0.1$ and $Q^2 > 0.3 \text{ GeV}^2$. Experimental analyses in DIS experiments need to know R down to measured values of x and for $0 < Q^2 < Q_{meas}^2$. Two phenomenological studies deliver estimates of R in the unmeasured region. Both the perturbative QCD contribution, which at low x and low Q^2 is dominated by the photon-gluon mechanism, and a non-perturbative term are there taken into account. In [50] the latter contribution is determined phenomenologically while in [48] it is fitted to the low Q^2 data.

3.3. Experimental data

The lowest values of x , correlated with lowest values of Q^2 ($x \sim 10^{-5}$ and $Q^2 \sim 0.001 \text{ GeV}^2$), were reached by the E665 Collaboration at Fermilab by applying a special experimental technique which permits the measurement of muon scattering angles as low as 1 mrad. At HERA the lowest values of Q^2 (1.5 GeV^2) were recently reached by two methods: shifting the interaction point in the proton beam direction in order to increase the acceptance of low Q^2 events and by using radiative events with hard photon emission collinear with the incident electron, Fig.2.5, [5]. The radiative events can be interpreted as non-radiative ones with reduced electron beam energy.

During the last three years an abundance of new data reaching Q^2 values smaller than 1 GeV^2 have appeared. These comprise: results on the proton and deuteron structure functions from NMC ($x > 0.006$, $Q^2 > 0.5 \text{ GeV}^2$) [64] Fig. 2.7, and E665 ($x > 0.0001$, $Q^2 > 0.2 \text{ GeV}^2$) [24] Fig. 2.8; results on the deuteron-to-proton structure function ratio, F_2^d/F_2^p , measured by NMC and E665 for $x > 0.0008$, $Q^2 > 0.2 \text{ GeV}^2$ (NMC [53, 65]) and $x > 0.000005$, $Q^2 > 0.004 \text{ GeV}^2$ (E665 [66, 26]), Fig. 2.10(left), precise results from these two collaborations on x , A and Q^2 dependence of nuclear shadowing [30, 32, 35, 31, 67, 34], Fig. 2.10(right) and Fig. 2.11; and measurements of $R^{Ca} - R^C$ [45], $R^d - R^p$ [46], Fig. 2.14(left), R^p and R^d at low x by NMC [47] and R^A at low x by CCFR [48].

The above-mentioned data were presented and discussed in Section 2. Here we shall add only a few remarks connected with their low Q^2 behaviour. The data on the nucleon F_2 display a weak x , and possibly a stronger than logarithmic Q^2 , dependence, at Q^2 lower than a few GeV^2 . Observe that also the photoproduction cross section between the fixed-target and HERA energies increases rather weakly with energy, cf. Fig. 2.6. This should be contrasted with measurements at HERA for Q^2 larger than a few GeV^2 , which show a strong increase of F_2 with decreasing x , Fig. 2.3. The QCD analysis of the NMC F_2 data, [39], show that the contribution of higher twists of the form similar to (3.4) is moderate even at scales about 1 GeV^2 . This is visible in Fig. 2.8 where the $F_2^p(x, Q^2)$ at low Q^2 is well described by models [23, 17] directly containing higher twist contributions. The higher twists seem also to account for the Q^2 dependence of the $F_2^p - F_2^n$ function, cf. section 2.6.

The F_2^d/F_2^p ratio, Fig. 2.10(left), which stays always below unity down to the smallest measured values of x , reflects nuclear shadowing in the deuteron, only weakly dependent on x . The data are well described by a model [27], which contains the VMD part, essential at low Q^2 , and which relates shadowing to the diffractively produced

final states. The agreement extends over nearly five orders of magnitude in x . No clear Q^2 dependence is visible in the shadowing data in a wide interval of Q^2 , neither in F_2^d/F_2^p nor in F_2^A/F_2^D [26, 34], cf. Fig. 2.11(right), except possibly for $F_2(Sn)/F_2(C)$ at $x < 0.1$, [35]. Shadowing thus appears as a leading twist phenomenon.

3.4. Outlook

In this section we have listed the ideas and results concerning the electroproduction structure functions in the region of low values of x and Q^2 . $F_2(x, Q^2)$ should vanish linearly with Q^2 for $Q^2 \rightarrow 0$ (for fixed ν), an important property which follows from the conservation of the electromagnetic current. The purely partonic description of inelastic lepton scattering has thus to break down for low Q^2 . At moderate Q^2 the higher twist contributions to F_2 which vanish as negative powers of Q^2 are sometimes included in the QCD data analysis. One also expects at low Q^2 that the VMD mechanism should play an important role.

The small x behaviour of $F_2(x, Q^2)$ is dominated by pomeron exchange. Analysis of the structure function in the small x region for both low and moderate values of Q^2 can clarify our understanding of the pomeron. At large Q^2 the problem is linked with the QCD expectations concerning deep inelastic scattering at small x [68]. Besides the structure functions (or total cross sections) complementary information on the pomeron can also be obtained from the analysis of diffractive processes in the electro- and photoproduction. This concerns both inclusive diffraction and diffractive production of vector mesons [69].

Descriptions of the low Q^2 , low x behaviour of F_2 range from pure fits to experimental data to dynamically motivated models.

There now exists a wealth of measurements of F_2 in the low Q^2 , low x region. These include the NMC and E665 results which extend down to very low x and Q^2 and display characteristic “approach to scaling” behaviour, as well as the first results from HERA at Q^2 which extend down to 1.5 GeV^2 . The data were QCD analysed, showing its applicability down to scales of the order of 1 GeV^2 . Nuclear shadowing was studied in great detail for targets ranging from $A = 2$ to $A = 208$ by the NMC and E665 collaborations. Its x , Q^2 and A dependence were precisely measured. Preliminary data on $R(x, Q^2)$ have also been reported (NMC and CCFR).

The fixed-target (unpolarised) structure function measurement programme comes to an end in 1996. Many experiments contributed in a great and successful effort to learn about properties of partons and strong interactions. Several aspects of this knowledge are yet not understood. One of these and perhaps the most challenging one is low x dynamics and in particular its dependence on the probing photon virtuality, Q^2 . The new possibilities concerning the study of this problem have opened up with the advent of HERA. The data collected there show a very strong increase of F_2 with decreasing x at high Q^2 . As the HERA data improve and extend to lower Q^2 it will be informative to see in which region of Q^2 the strong increase gives way to the slow rise evident in photoproduction, see Fig. 2.6. Such data in the transition region open up the possibility of a unified understanding of the underlying dynamics.

4. QCD interpretation

4.1. Introduction

The behaviour of the proton structure function $F_2(x, Q^2)$ at small x reflects the behaviour of the gluon distribution, since the gluon is by far the dominant parton in this regime. Fig. 4.1 shows a sketch of the gluon content of the proton in the various kinematic regions. Perturbative QCD does not predict the absolute value of the parton distributions, but rather determines how they vary from a given input. For instance from given initial distributions at some scale Q_0^2 , Altarelli-Parisi (GLAP) [4] evolution enables us to determine the distributions at higher Q^2 . GLAP evolution resums the leading $\alpha_S \ln(Q^2/Q_0^2)$ terms where, in a physical gauge, the $\alpha_S^n \ln^n(Q/Q_0^2)$ contribution is associated with a space-like chain of n gluon emissions in which the successive gluon transverse momenta are strongly ordered along the chain, that is $q_{T1}^2 \ll \dots \ll q_{Tn}^2 \ll Q^2$.

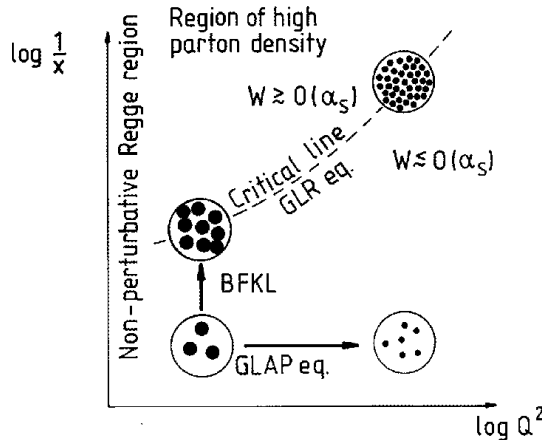


Figure 4.1. The gluon content of the proton as “seen” in various deep inelastic (x, Q^2) regimes. The critical line, where gluon recombination becomes significant, occurs when $W \approx O(\alpha_S)$. W is the ratio of the quadratic recombination term to the term linear in the gluon density which occur on the right hand side of the evolution equation.

At sufficiently high electron-proton c.m. energy \sqrt{s} we encounter a second large variable, $1/x \sim s/Q^2$, and we must resum the leading $\alpha_S \log(1/x)$ contributions. The resummation is accomplished by the BFKL equation [2]. In this case we have no ordering in q_{Ti}^2 along the chain, but rather, as we evolve to smaller x , we have a diffusion or random walk in $\ln q_{Ti}^2$. The lack of strong ordering means that we have to work in terms of the gluon distribution $f(x, k_T^2)$ unintegrated over the gluon transverse momentum k_T . As we proceed to smaller x , via the BFKL equation, the gluon density f is predicted to increase as $x^{-\lambda}$ with $\lambda \sim 0.5$ (on account of the increased q_{Ti} phase space) and to possess a Gaussian-type distribution in $\ln k_T^2$ which broadens as $\sqrt{\ln(1/x)}$. This singular type of growth in x , accompanied by the diffusion in $\ln k_T^2$, is the characteristic property of the BFKL gluon density $f(x, k_T^2)$.

The increase of the gluon density with decreasing x cannot proceed indefinitely. Eventually we reach the critical line where gluon recombination effects become appreciable, see Fig. 4.1. At the onset these effects can be estimated by perturbative

QCD, but finally we enter a region of high density of weakly interacting partons, where we have the unusual situation in which we cannot use the normal methods of perturbation theory even though α_S is small — a region of much speculation and interest. At higher Q^2 we can evolve further in x before we reach the critical line, since the resolution goes as $1/Q$ and the transverse area occupied by a parton $\sim 1/Q^2$.

4.2. GLAP-based descriptions at small x

Traditionally the parton distributions of the proton are determined by global fits to a wide range of deep inelastic and related data, see the review in these proceedings [70]. The starting distributions are parametrized at some scale Q_0^2 , typically $Q_0^2 = 4 \text{ GeV}^2$, and evolved up in Q^2 using next-to-leading order GLAP evolution. The parameters are then determined by fitting to all the available data. A wide range of precise data exist for $x \gtrsim 0.05$ and so the partons are well constrained in this region.

On the other hand for small x , $x \sim 10^{-3}$, only the structure function $F_2(ep)$ is measured. In principle these HERA data should determine the small x behaviour of the gluon and the sea quark distributions. Roughly speaking the data on F_2 constrain the sea S and the data on the slope $\partial F_2/\partial \ln Q^2$ determine the gluon g . For example if we take

$$F_2 \sim xS \sim A_S x^{-\lambda_S} \quad (4.1)$$

$$\frac{\partial F_2}{\partial \ln Q^2} \sim xg \sim A_g x^{-\lambda_g}, \quad (4.2)$$

then we might expect to determine λ_S and λ_g . The most recent HERA data are well described by a parametrization with $\lambda_S = \lambda_g \sim 0.2 - 0.25$ with $Q_0^2 = 4 \text{ GeV}^2$, see MRS(A') [15]. However, as the data improve we should be able to determine λ_S and λ_g independently. To be more precise the slope (4.2) gives information on $P_{qg} \otimes g$. The convolution means that the gluon is sampled at higher x . We will see the convolution also has implications for the scheme dependence.

A satisfactory description of the data is also obtained from a set of “dynamical” partons evolved up from valence-like distributions at a much lower scale $Q_0^2 = 0.34 \text{ GeV}^2$ [14]. The dynamical model was originally based on the attractive hypothesis that at some low scale we just have the u and d valence quark distributions. The gluon and sea quark distributions are generated radiatively from the valence quark distributions, via the processes $q \rightarrow qg$ and $g \rightarrow q\bar{q}$. Unfortunately the radiated distributions are spiked towards small x and must be supplemented by inputting a contribution at larger x . For instance to describe prompt photon data valence-like gluons are needed at the input scale Q_0^2 , and to describe the NMC measurements of F_2 valence-like sea quark distributions are required. It can be argued that $Q_0^2 = 0.34 \text{ GeV}^2$ is much too low for perturbative QCD to be reliable. The GRV philosophy is that GLAP evolution preserves the leading twist and so the parametrization becomes physical at some higher scale. The surprise is that the GRV partons appear to give a reasonable description as low as $Q^2 \approx 1 \text{ GeV}^2$.

An idea of the potential steepness of the gluon distribution within GLAP evolution can be glimpsed from the double leading logarithm (DLL) approximation which applies at small x and large Q^2/Q_0^2 [71]. In this limit GLAP evolution of the gluon gives

$$xg(x, Q^2) \sim xg(x, Q_0^2) \exp \left(2 \left[\frac{36}{25} \ln \left(\frac{t}{t_0} \right) \ln \left(\frac{1}{x} \right) \right]^{\frac{1}{2}} \right) \quad (4.3)$$

where $t \equiv \ln(Q^2/\Lambda^2)$. That is, xg increases faster than any power of $\ln(1/x)$, but slower than a power of $(1/x)$. Moreover we see that xg increases faster as $x \rightarrow 0$ the longer is the $Q_0^2 \rightarrow Q^2$ evolution. The GRV analysis demonstrates that with a flat (or, to be precise, a decreasing) input distribution at small x such a rise is obtained with the low starting point $Q_0^2 = 0.34 \text{ GeV}^2$. The origin of the growth of (4.3) at small x can be traced back to the singular behavior of the gluon anomalous dimension at $n = 1$ or $\omega = 0$ (see below). On the other hand, if the input gluon is singular, $xg(x, Q_0^2) \sim x^{-\lambda}$ with $\lambda > 0$, as in MRS/CTEQ, then this behaviour overrides the DLL form. In fact the present HERA data for F_2 cannot really distinguish between these small x gluon behaviours. The data are shown in Fig. 2.4 as a function of $\ln Q^2$ at given values of x . From (4.2) we see that the slope of these points is a measure of the gluon. Also shown on the plot is the description obtained from GRV partons [14]. The GRV prediction is a little too steep at small x but this could be easily accommodated by a small increase in Q_0^2 . In summary the existing data determine only one parameter; either $\lambda (\approx 0.2 - 0.25)$ of the MRS/CTEQ global fits or $Q_0^2 (\approx 0.5 - 1 \text{ GeV}^2)$ of the GRV-type description.

In principle, a possible check of whether the rise of F_2 at small x is closer to the behaviour (4.3) or to a power-like growth may be obtained from the double asymptotic scaling behaviour [72]. Namely, (4.3) suggests that, instead of the variables $\ln(1/x)$ and $\ln(t/t_0)$, one might use the two variables

$$\sigma = \sqrt{\ln(t/t_0) \ln(x_0/x)}, \quad \rho = \sqrt{\ln(t/t_0) / \ln(x_0/x)}. \quad (4.4)$$

For example, by rescaling the observed F_2 by a factor R'_F which eliminates power-like prefactors to the exponential in (4.3) and higher order corrections in the exponent the remainder should be proportional to the exponential, i.e. the logarithm of $R'_F F_2$ should be linear in σ and independent of ρ . Data [73] show approximate agreement with this prediction, provided the scale Q_0^2 is chosen to be 1 GeV^2 and $x_0 \sim 0.1$. The resummation of $\alpha_S \ln(1/x)$ contributions will, at sufficiently small x , give effects which violate the double scaling form.

There is, however, some warning against the use of next-to-leading order GLAP evolution in combination with a flat input for explaining the observed rise at small x . Consider, for simplicity, GLAP evolution for the gluon alone

$$\frac{\partial g(x, Q^2)}{\partial \ln Q^2} = \int_x^1 \frac{dy}{y} P_{gg} \left(\frac{x}{y} \right) g(y, Q^2). \quad (4.5)$$

In moment space this takes the factorized form

$$\frac{\partial \bar{g}(\omega, Q^2)}{\partial \ln Q^2} = \gamma_{gg}(\omega, \alpha_S) \bar{g}(\omega, Q^2) \quad (4.6)$$

where the anomalous dimension in leading order near $\omega = 0$

$$\gamma_{gg} \equiv \int_0^1 dx x^\omega P_{gg}(x, \alpha_S) \approx \frac{\bar{\alpha}_S}{\omega} \quad (4.7)$$

In x -space this approximation is equivalent to retaining only the small x approximation $P_{gg} \approx \bar{\alpha}_S/x$ with $\bar{\alpha}_S \equiv 3\alpha_S/\pi$. This is the DLL approximation which generates a gluon distribution of the form given in (4.3). The general pattern of the terms that occur in the expansion of the anomalous dimensions and the coefficient function functions as power series in α_s and the moment index ω is summarised in Fig. 4.2.

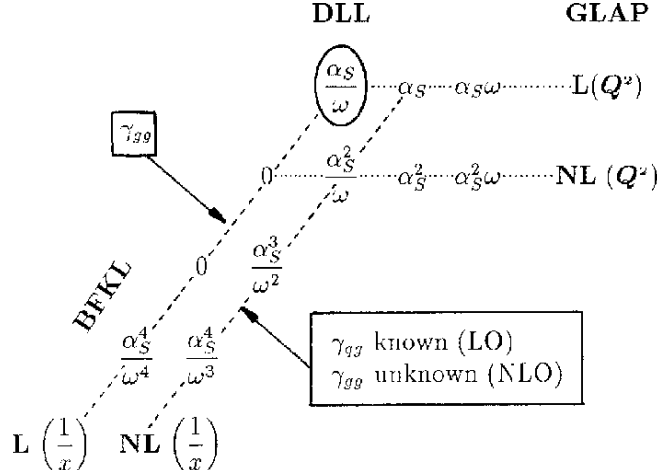


Figure 4.2. Possible terms in the perturbative expansion of the anomalous dimensions (and coefficient functions). Leading order GLAP and BFKL evolution have only the DLL term in common.

The terms that are included in the full leading (and next-to-leading) order GLAP evolution are shown connected by horizontal dotted lines. On the other hand in the vicinity of the point $\omega = 0$ which governs the small x limit it will be more accurate to resum, in the anomalous dimension, all singular terms of the form

$$\gamma_{gg} \approx \sum_{n=1}^{\infty} A_n \left(\frac{\alpha_S}{\omega} \right)^\omega \quad (4.8)$$

which in x -space corresponds to

$$\sum_{n=1} A_n \alpha_S \frac{(\alpha_S \log 1/x)^{n-1}}{(n-1)!}, \quad (4.9)$$

that is an ω^{-n} behaviour translates into a $(\log 1/x)^{n-1}$ behaviour. These terms are included in the BFKL equation, and the coefficients A_n have been computed [74]. Interestingly the coefficients $A_2 = A_3 = A_5 = 0$. The anomalous dimension γ_{gg} has a similar structure as γ_{qq} , i.e. the leading order consists of terms $(\alpha_s/\omega)^n$, whereas for γ_{qq} and γ_{qg} the most singular terms are down by one power of α_s : $\alpha_s(\alpha_s/\omega)^n$. For all four cases the coefficients of these leading order terms are known. In particular, for γ_{qq} the coefficients are non-vanishing (unlike γ_{gg}), positive definite and large [75]. As a consequence the BFKL increase† of $F_2(\sim P_{qq} \otimes g)$ with decreasing x appears to be much more due to the resummation in P_{qq} (and in the coefficient functions) than that for $g(\sim P_{gg} \otimes g)$. It is clear that for a consistent analysis we need higher order corrections to γ_{gg} and γ_{qg} : terms of the order $\alpha_s(\alpha_s/\omega)^n$. It is hoped that they can be derived from the next-to-leading order corrections to the BFKL kernel which are being computed by Fadin and Lipatov [77].

† The reduction of the BFKL k_T -factorized (4.14) to the GLAP collinear form is discussed in ref. [76].

Based upon our present (limited) knowledge of these singular terms of the matrix of anomalous dimensions several numerical studies have been undertaken [78], incorporating resummation in various ways. A general conclusion is that GLAP evolution with a flat input distribution is rather sensitive to whether resummation of the singular terms is included or not. The resummation in γ_{qg} , although formally nonleading, seems to play a key role. On the other hand, if we start from a singular $x^{-\lambda}$ input with $\lambda \gtrsim 0.3$ then the result appears to be rather stable with respect to resummation. A theoretical issue is the scheme dependence of the resummation effects. Catani and Hautmann emphasized at the Workshop that accurate data on F_L could remove the ambiguities and overconstrain the problem. Indeed they showed that it is possible to obtain scheme independent evolution equations of the form

$$\begin{aligned} \frac{\partial F_2(x, Q^2)}{\partial \ln Q^2} &\sim \Gamma_{22} \otimes F_2 + \Gamma_{2L} \otimes F_L \\ \frac{\partial F_L(x, Q^2)}{\partial \ln Q^2} &\sim \Gamma_{L2} \otimes F_2 + \Gamma_{LL} \otimes F_L \end{aligned}$$

which inter-relate only physical observables, where the anomalous dimensions Γ_{ij} are computable in perturbative QCD.

4.3. BFKL-based description of F_2 at low x

This topic is well reviewed in [68], so we will be brief. The BFKL equation for the unintegrated gluon distribution $f(x, k_T^2)$ may be written in the differential form

$$\frac{\partial f(x, k_T^2)}{\partial \ln(1/x)} = \frac{3\alpha_S}{\pi} k_T^2 \int \frac{dk_T'^2}{k_T'^2} \left[\frac{f(x, k_T'^2) - f(x, k_T^2)}{|k_T'^2 - k_T^2|} + \frac{f(x, k_T^2)}{(4k_T'^4 + k_T^4)^{\frac{1}{2}}} \right] \quad (4.10)$$

$$\equiv K \otimes f \quad (4.11)$$

where the $f(x, k_T'^2)$ term corresponds to real gluon emissions, and where the cancellation of the $k_T' = k_T$ singularity between the real and virtual gluon contributions is apparent. The gluon distribution $f(x, k_T^2)$ may be calculated by integrating down in x from a starting distribution at, say, $x = x_0 = 0.01$. The BFKL equation effectively sums the leading $\alpha_S \log(1/x)$ contributions; from (4.11) we see that as $x \rightarrow 0$

$$f \sim \exp(\lambda \log(1/x)) \sim x^{-\lambda} \quad (4.12)$$

where λ is the largest eigenvalue of the BFKL kernel K . For fixed α_S it can be shown [2] to be $\lambda = (3\alpha_S/\pi) 4 \ln 2$. We need to know the NLO $\log(1/x)$ contributions to fully specify the running of α_S . However, if a physically reasonable prescription for the running is assumed then it is found [79] that the solution has the form

$$f \sim C(k_T^2) x^{-\lambda}. \quad (4.13)$$

For running α_S the integral in (4.10) is weighted more to the infrared (non-perturbative) region, but it is found that $\lambda \approx 0.5$ is less sensitive to the treatment of the infrared region than the normalization C .

The BFKL predictions of the proton structure functions F_i are obtained using the k_T factorization theorem [80, 81, 82]

$$F_i(x, Q^2) = \int_x^1 \frac{dx'}{x'} \int \frac{dk_T'^2}{k_T'^2} f(x', k_T'^2) F_i^{\gamma g} \left(\frac{x}{x'}, k_T'^2, Q^2 \right) \quad (4.14)$$

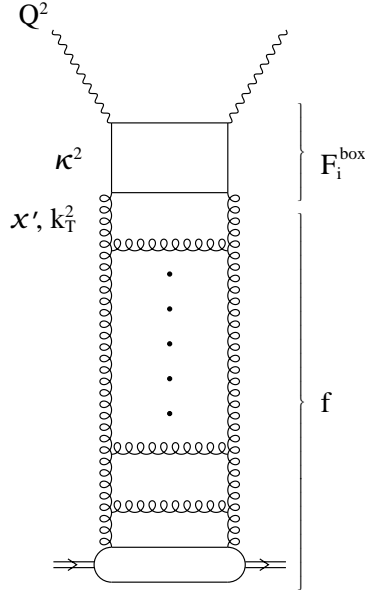


Figure 4.3. Pictorial representation of the k_T -factorization formula of (4.14). The variables x' and k_T that are integrated over are, respectively, the longitudinal fraction of the proton's momentum and the transverse momentum carried by the gluon which dissociates into the $q\bar{q}$ pair.

where $F_i^{\gamma g}$ are the off-shell gluon structure functions which at lowest order are given by the quark box (and crossed-box) contributions to photon-gluon fusion, see Fig. 4.3. In the small x region it is clearly important to tackle the resummation of the $\alpha_S \log(1/x)$ contributions and to go beyond (next-to-leading order) GLAP. Indeed a satisfactory BFKL prediction of the rise of F_2 at small x was obtained prior to the HERA measurements [79]. However, there are ambiguities and limitations in the BFKL description of F_2 . We list them below.

- (i) Due to the diffusion of the gluon distribution $f(x, k_T^2)$ in $\ln k_T^2$, there is a significant contribution to (4.14) from the infrared region which is beyond the scope of perturbative QCD and has to be included phenomenologically. The ambiguity is primarily in the overall normalization of F_2 rather than the x dependence. A physically reasonable choice of the infrared parameters is found to give the experimental normalization.
- (ii) The BFKL equation only resums the leading order $\ln(1/x)$ terms. The next-to-leading order contributions are essential for a stable prediction. Sub-leading effects, including energy-momentum conservation on the gluon emissions, are expected to suppress the value of λ , see, for example, [83]. When known, these will check whether or not the $\alpha_S(k_T^2)$ prescription for the running of α_S is correct.
- (iii) An underlying soft Pomeron contribution has to be included in the small x region, determined by extrapolation of the large x values of F_2 .
- (iv) Shadowing corrections to the BFKL equation will eventually suppress the $x^{-\lambda}$ growth. Although they have not yet been fully formulated, the evidence from the

observed ratio of diffractive to non-diffractive deep inelastic events, and from the persistent rise of F_2 at very low $Q^2 \approx 2 \text{ GeV}^2$, indicates that shadowing effects are at most 10% in the HERA regime.

- (v) We need a unified approach which incorporates both the BFKL and GLAP resummations. We discuss recent developments below.

The BFKL gluon distribution f is characterised by a steep rise with decreasing x which is accompanied by a diffusion in $\ln k_T^2$. F_2 measures only the rise; it is too inclusive an observable to probe the k_T dependence. For this we need to explore the properties of the final state, such as deep inelastic events containing an identified energetic forward jet, see section 5.

4.4. Unified evolution

Because of the possible onset of the BFKL behaviour of F_2 in the HERA small x domain it is important to study the validity of the GLAP evolution in this region and to look for an interpolation between the two approaches. First answers to these questions are contained in the studies of resummation effects (see above). Including the $\log(1/x)$ resummation effects in GLAP, via the $(\alpha_S/\omega)^n$ and $\alpha_S(\alpha_S/\omega)^n$ terms in γ_{gg} and γ_{qg} respectively (and also in the coefficient functions) leads to a stronger increase of F_2 at small x , i.e. we are getting closer to BFKL.

Ciafaloni, Catani, Fiorani, and Marchesini [84] have proposed a unified evolution equation which embodies BFKL evolution at small x and GLAP evolution at larger x (see also the review in these proceedings [68]). The CCFM equation is based on the coherent radiation of gluons, which leads to an angular ordering of gluon emissions. Outside the ordered region there is destructive interference between the emissions. For simplicity we concentrate on small x . Then the differential probability for emitting a gluon of momentum q is of the form

$$dP \sim \bar{\alpha}_S \Delta_R \frac{dz}{z} \frac{d^2 q_T}{\pi q_T^2} \Theta(\theta - \theta') \quad (4.15)$$

where successive emissions along the space-like gluon chain occur at larger and larger angles. Δ_R represents the virtual gluon loop corrections which screen the $1/z$ singularity. We can use (4.15) to obtain a recursion relation expressing the contribution of the n gluon emission in terms of that of $n - 1$. On summing we find that the gluon distribution satisfies an equation

$$F(x, k_T^2, Q^2) = F^{(0)}(x, k_T^2, Q^2) + \quad (4.16)$$

$$\bar{\alpha}_S \int_x^1 \frac{dz}{z} \int \frac{d^2 q}{\pi q^2} \Delta_R \Theta(Q - zq) F\left(\frac{x}{z}, |\vec{k}_T + \vec{q}|^2, q^2\right)$$

where $F = f/k_T^2$. The angular ordering, in the form of the Θ function, introduces a dependence on an additional scale (that turns out to be the hard scale Q of the probe), which is needed to specify the maximum angle of gluon emission.

When we “unfold” Δ_R , so that the real and virtual contributions appear on equal footing, and then take the leading $\ln(1/x)$ approximation we find that (4.17) reduces to the BFKL equation with F independent of Q^2 (since $\Theta(Q - zq) \rightarrow 1$). On the other hand, in the large x region $\Delta_R \sim 1$ and $\Theta(Q - zq) \rightarrow \Theta(Q - q)$, which leads to GLAP transverse momentum ordering. If we then replace $\bar{\alpha}_S/z$ by P_{gg} we see that (4.17) becomes the integral form of the GLAP equation.

Explicit numerical solutions $F(x, k_T^2, Q^2)$ of the CCFM equation have recently been obtained in the small x region [85]. As anticipated, they show a singular $x^{-\lambda}$ behaviour, with $\lambda \approx 0.5$, a k_T dependence which broadens as x decreases and a suppression of the gluon as compared to BFKL at low Q^2 . Fig. 4.4 shows a comparison of the CCFM k_T -factorization prediction for $F_2 = F \otimes F_2^g$ with recent HERA data. The DLL dot-dashed curve is obtained by the same procedure except that we replace $\Theta(Q - zq)$ by $\Theta(Q - q)$ and set $\Delta_R = 1$. The difference between the CCFM and DLL curves therefore show the value of x at which resummation effects become important.

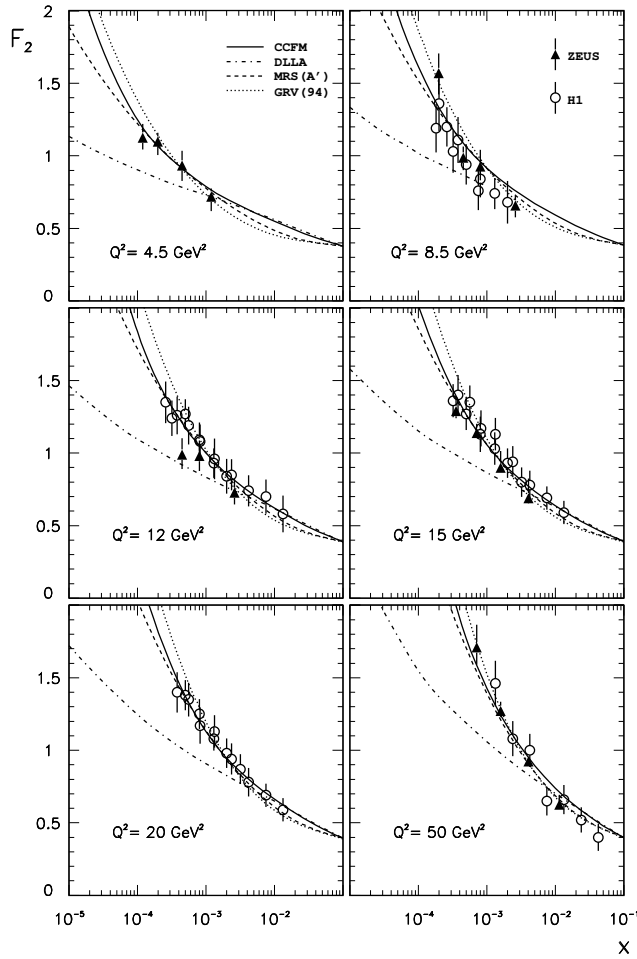


Figure 4.4. The continuous curve is the CCFM prediction of F_2 obtained in ref. [86] compared with preliminary 1994 HERA measurements [87]. The DLL curve is obtained by the same procedure except that we replace $\Theta(Q - zq)$ by $\Theta(Q - q)$ and set $\Delta_R = 1$. Also shown are the descriptions obtained by GRV [14] and MRS(A') [15] partons. The figure is taken from ref. [86].

4.5. Open questions

A completely satisfying explanation of the observed rise at small x cannot avoid investigating the transition from the structure function F_2 at small x to the photoproduction cross section at high energies. Approaching this transition from the deep inelastic kinematic region (large Q^2 and not so small x) where perturbative QCD can safely be used, we expect first to see the onset of more complicated partonic interactions (e.g. recombination effects) which will screen the strong rise of the GLAP or BFKL approximation. So far, these contributions have not been observed. Numerical studies based upon the nonlinear Gribov-Levin-Ryskin [88] equation indicate that in the HERA region it will be difficult to identify the screening effects: even if they are not negligibly small in the HERA region, they could be masked by a change in the input to the GLAP evolution equations. Unfortunately, the GLR equations cannot be used to make a reliable quantitative prediction of the magnitude of screening effects, due primarily to the lack of knowledge of the characteristic transverse area within which the gluons are concentrated [89], but also of the size of the enhancement due to QCD multigluon correlations [90, 91]. So at present it is not quite clear yet whether recombination effects are relevant at HERA and how large they are.

The conventional GLAP analysis is constrained to leading twist only, and for large Q^2 this approximation is well-justified. However, once we are approaching the low- Q^2 region, the neglect of higher-twist becomes more and more questionable. Interestingly the BFKL Pomeron does include higher-twist contributions, but only a small subset of the higher-twist operators that exist in QCD. In the small- x region, among the twist-four operators it is the four gluon operator which is expected to become important. Evolution equations of higher-twist operators have been studied in [92], and the anomalous dimension of the twist-four gluon operator has been calculated in [93, 91]. But so far, the results of these QCD calculations have not been used yet for numerical studies. A phenomenological estimate of higher twist contributions at small x and low Q^2 has been done in [63]: it indicates that higher-twist effects are surely important when Q^2 less than 1 GeV², and when Q^2 increases that they disappear, for large x more rapidly than for small x . Further studies of higher twist contributions at small x are important and clearly needed.

It is quite clear that we are still quite far away from a satisfactory understanding of the small- x regime. The measurements of F_2 at small x have considerably improved and indicate a fairly rapid transition from the “soft” $x^{-0.08}$ behaviour at $Q^2 = 0$ to a more singular $x^{-0.2}$ behaviour by $Q^2 \sim 2$ GeV². Acceptable GLAP-based partonic descriptions (including next-to-leading order $\log Q^2$ terms) are possible down to at least $Q^2 \sim 1$ GeV². Equally well the small x data can be described by BFKL leading order $\alpha_S \log(1/x)$ resummation, via k_T factorization; though we await the next-to-leading $\log(1/x)$ contribution for a stable prediction. We must develop a unified formalism which embraces both GLAP and BFKL. The CCFM approach is a step in this direction. As noted above, more work is needed to quantify the effects of parton screening. Of course the partonic formalism must eventually fail as we go to lower and lower Q^2 . It remains a challenge to match this perturbative QCD approach to the successful non-perturbative Regge and Vector-Meson-Dominance description of proton structure for $Q^2 \sim 0$.

5. Hadronic Final States

In order to make further progress to find the appropriate QCD approach to use in the small x regime, hadronic final states are analysed. The experiments at HERA measure the full hadronic final state, apart from losses in the beampipe. Several results on hadronic final states are reported in [41]. In this section three topics will be addressed. The first topic is charged particle spectra as measured in the current region of the Breit frame. Here one would expect the timelike evolution of the parton shower to evolve as in e^+e^- annihilation. The second topic is the study of strangeness production and a possible discrepancy of the strangeness suppression factor between DIS and e^+e^- experiments. Strange particle data can also be interpreted in the light of possible signals for instanton production. Finally an overview of the hadronic final state at low x will be given with a discussion of possibilities of detecting the onset of QCD $\alpha_S \log 1/x$ resummation effects.

5.1. Breit frame: current region

A natural frame to study the dynamics of the hadronic final state in DIS is the Breit frame [94]. In the Quark Parton Model (QPM) the z -component of the momentum of the incoming quark is $Q/2$ before and $-Q/2$ after the interaction with the exchanged virtual boson. In e^+e^- annihilation the two quarks are produced with equal and opposite momentum, $\pm\sqrt{s}/2$. In the direction of the struck quark (called the current region) in the Breit frame the particle spectra are expected to have no dependence on x and a dependence on Q^2 similar to that observed in e^+e^- annihilation [95] at energy $s = Q^2$.

Both ZEUS [96] and H1 [97] have published results of the charged particle scaled momentum and multiplicity spectra in the current region of the Breit frame. The results indicate these fragmentation properties of the struck quark in DIS are similar to those from quarks created in e^+e^- annihilation for $Q^2 > 60 \text{ GeV}^2$. For $Q^2 < 60 \text{ GeV}^2$ the mean multiplicity, $\langle n_{ch} \rangle$, tends to be lower in DIS than in e^+e^- experiments [98], see Fig. 5.1.

In the low Q^2 regions measured at HERA it is possible to study the x dependency by comparisons with data from previous fixed-target DIS measurements [99], which are 2 orders of magnitude higher in x than the values probed at HERA. In Fig. 5.1 it is shown that the DIS $\langle n_{ch} \rangle$ data exhibit a marked dependence on x contrary to the naive expectation. Also, in this higher x region the agreement between DIS and e^+e^- experiments seems to hold. This x dependence can be explained when mass effects are taken into account in the DIS kinematics. For (2+1) jet kinematics, the longitudinal momentum of the outgoing quark pair is given by $p_Z^{rad} = \frac{1}{2}(\hat{s} - Q^2)/Q$ where \hat{s} is the square of the invariant mass of the emitted $q\bar{q}$ or a qg pair. When $Q^2 \gg \hat{s}$, the radiation is emitted in the QPM direction, $p_Z^{rad} \sim p_Z^{QPM}$. However, at low Q^2 and x , \hat{s} is likely to be bigger than Q^2 and the radiation will be emitted in the direction opposite to the QPM direction, hence depopulating the current region. Typically the smallest resolvable value of \hat{s} is around 20 GeV^2 in the kinematic region of HERA, therefore at Q^2 around 10 GeV^2 the emitted radiation has a $p_Z^{rad} = Q/2$ or more, whereas $p_Z^{QPM} = -Q/2$.

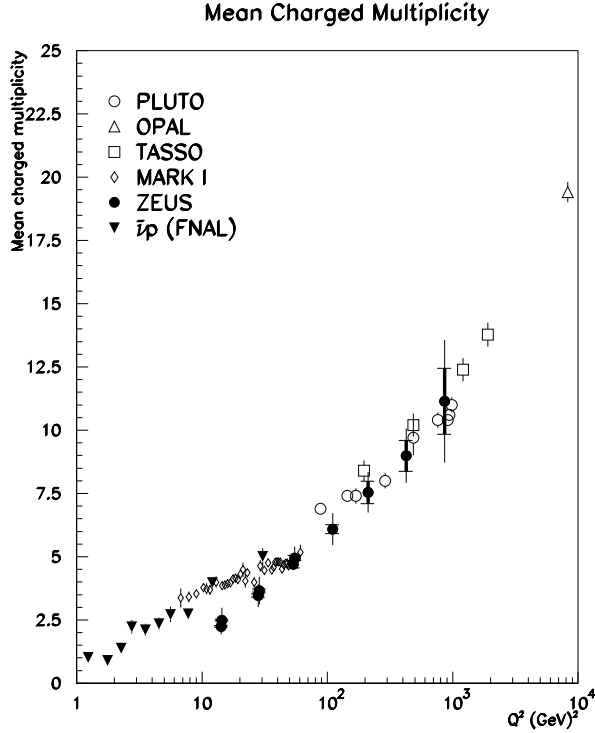


Figure 5.1. Twice the measured ZEUS multiplicity in the current region is compared to the results from HRS, MARK I, OPAL, PLUTO and TASSO. Also show is twice the current region multiplicity from FNAL DIS $\bar{\nu}P$ experiment. All data have been corrected for K_S^0 and Λ decays.

5.2. Strangeness Production

The production of strangeness has been studied by the experiments at HERA through the production of K^0 mesons and Λ baryons [100, 101]. These particles are reconstructed from the measurements of the charged tracks of the decay particles. The acceptance is presently limited to the central region of the detectors, i.e. in pseudorapidity η $|\eta| < 1.3$, hence the strangeness production measurement mainly covers from the current quark fragmentation region. Fig. 5.2 shows K^0 multiplicities, corrected for detector effects, for non-diffractive deep inelastic events (i.e. events with no visible gap in the direction of the proton remnant, see [43]) as function of the pseudorapidity η and the transverse momentum p_t . The data are compared with model predictions. The MEPS model is based on the LEPTO [102] program and contains first order QCD matrix elements, matched with parton showers which approximate the higher orders, for the partonic simulation of the hadronic final state. The CDM model is based on the ARIADNE [103] program and provides an implementation of the colour dipole model of a chain of independently radiating dipoles formed by emitted gluons (photon gluon fusion events are not described by this picture and are added at a rate given by the QCD matrix elements). The calculations are shown for standard strange quark suppression of 0.3, i.e. the production of quark-antiquark pairs is $u\bar{u} : d\bar{d} : s\bar{s} = 1 : 1 : 0.3$, tuned essentially on e^+e^- hadronic data. It appears

that this predicts to many K^0 's, as is seen most prominently in the η distribution. The calculation with a strangeness suppression of 0.2 is in better agreement with the data.

This difference is intriguing and could be a sign of the breakdown of jet universality, e.g. due to a “medium dependence” of the fragmentation, or different kind of gluon strings in e^+e^- and ep scattering [104]. However before speculating on such possibilities, additional data are needed. It should be checked whether it is the K^0 rate which is lower, or whether all particle rates are affected, e.g. by studying K/π ratios. Other strange particle species, especially anti-baryons, should be studied as well.

Strange particle production is also of interest for the study of QCD instantons. Instantons are related to non-perturbative effects of QCD, and effects on the hadronic final state in ep collisions at HERA were recently calculated [105]. Due to the expected isotropic decay of a dense partonic system, events with an unusual structure are expected. The uncertainty on the expected instanton rate is however large. Due to the flavour symmetry in the instanton decay, less strangeness suppression is expected, leading to an average density of 0.4 K^0 's per unit of pseudorapidity in the region of the instanton [106]. The shape of the rapidity distribution is expected to be different from DIS events without an instanton. Clearly enhanced strangeness production will be one of the features to search for instantons, others being large E_T in a limited rapidity interval, isotropically spread energy, etc. Searching for instantons is one of the exciting topics of hadronic final state studies at HERA.

5.3. Tests of QCD in the small x regime

In Section 2 it was shown that the the proton structure function F_2 exhibits a strong rise towards small Bjorken- x . Originally, this rise caused much debate on whether the HERA data are still in a regime where the QCD evolution of the parton densities can be described by the GLAP [4] evolution equations, or whether they extend into a new regime where the QCD dynamics is described by the BFKL [2] evolution equation, but it was pointed out in Section 4 that present F_2 measurements do not yet allow us to distinguish between BFKL and conventional GLAP dynamics, and are perhaps too inclusive a measure to be a sensitive discriminator. Hadronic final states are expected to give additional information and could be more sensitive to the parton evolution.

For events at low x , hadron production in the region between the current jet and the proton remnant is expected to be sensitive to the effects of the BFKL or GLAP dynamics. At lowest order the BFKL and GLAP evolution equations effectively resum the leading logarithmic $\alpha_S \ln 1/x$ or $\alpha_S \ln Q^2$ contributions respectively. In an axial gauge this amounts to a resummation of ladder diagrams of the type shown in Fig. 5.3. This shows that before a quark is struck by the virtual photon, a cascade of partons may be emitted. The fraction of the proton momentum carried by the emitted partons, x_i , and their transverse momenta, k_{T_i} , are indicated in the figure. In the leading log Q^2 GLAP scheme this parton cascade follows a strong ordering in transverse momentum $k_{T_n}^2 \gg k_{T_{n-1}}^2 \gg \dots \gg k_{T_1}^2$, while there is only a soft (kinematical) ordering for the fractional momentum $x_n < x_{n-1} < \dots < x_1$. In the BFKL scheme the cascade follows a strong ordering in fractional momentum $x_n \ll x_{n-1} \ll \dots \ll x_1$, while there is no ordering in transverse momentum. The transverse momentum follows a kind of random walk in log k_T space: the value of k_{T_i} is close to that of $k_{T_{i-1}}$, but it can be both larger or smaller.

H1 PRELIMINARY

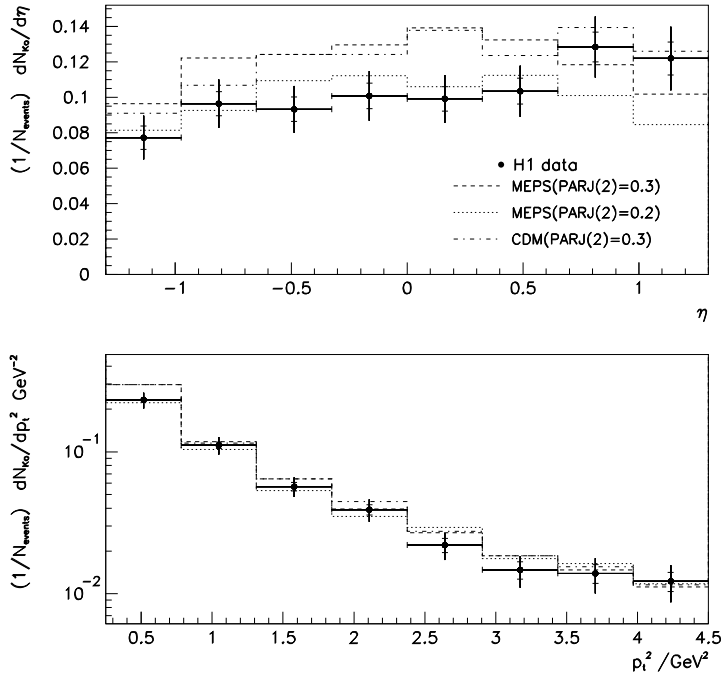


Figure 5.2. Corrected K^0 multiplicities in non-diffractive deep inelastic scattering events as a function of η (top) and p_t^2 (bottom) compared to the predictions of the MEPS and CDM Monte Carlo program. The inner error bars are statistical and the outer error bars contain the full statistical and systematical errors.

Several measurements of the hadronic final state have been suggested to exploit this difference at the parton level. The idea is to find observables which may reflect both of the BFKL characteristics of the unintegrated gluon distribution $f(x, k_T^2)$, that is the $x^{-\lambda}$ growth and the diffusion in $\log k_T^2$, as x decreases. Here we discuss those two measurements for which new information was provided during the Workshop: first, in section 5.4, we study the transverse energy (E_T) flow in the region away from the current quark jet and second, in section 5.5, we investigate the distribution of deep inelastic events containing an identified forward jet, that is, a measured jet as close as possible to, but distinct from, the proton remnants.

Apart from numerical calculations, predictions for final state observables are also available as Monte Carlo models, based upon QCD phenomenology. The CDM model description of gluon emission is similar to that of the BFKL evolution, because the gluons emitted by the dipoles do not obey strong ordering in k_T [107]. The CDM does not explicitly make use of the BFKL evolution equation, however. The MEPS model is based on GLAP dynamics; the emitted partons generated by the leading log parton showers are strongly ordered in k_T .

5.4. Energy flow in the central region

Due to the absence of k_T ordering the BFKL approach is expected to give a larger transverse energy, E_T , in the hadronic final state in the central region of the hadronic

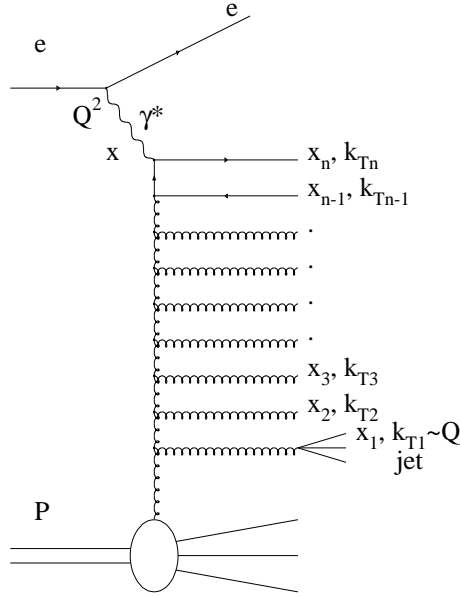


Figure 5.3. Parton evolution in the ladder approximation. The selection of DIS events containing a forward jet is illustrated.

centre-of-mass than the GLAP approach at low x . This corresponds to the very forward region of the detectors in the HERA laboratory frame. In this central region of the hadronic center-of-mass Golec-Biernat *et al*, [108] show using the GLAP approach that the partonic mean E_T , $\langle E_T \rangle$, increases with increasing x , while for BFKL the reverse is true, $\langle E_T \rangle$ decreases with increasing x . It should be noted though that the E_T spectra are difficult to calculate in the GLAP framework because the E_T weighting emphasizes unsafe regions of phase space.

Fig. 5.4 shows the transverse energy flow as a function of pseudorapidity, η , in the laboratory frame as measured by both H1 [109] and ZEUS [110]. The level of E_T is almost flat at ≈ 2 GeV/(unit of η). Also shown are the partonic calculations from [108] which seem to indicate a preference towards the BFKL approach over GLAP. Fig. 5.5 shows the mean transverse energy in the pseudorapidity range (as measured in the hadronic center-of-mass system) $-0.5 < \eta^* < 0.5$ by H1 [109]. The data exhibit a rise in $\langle E_T \rangle$ with decreasing x as can also be seen from the BFKL partonic calculations shown in the same figure. To definitively comment on whether these plots are signatures for BFKL it is necessary to understand the underlying hadronisation.

In order to investigate hadronisation effects in this region two Monte Carlo generators have been studied: the CDM model (labeled ARIADNE 4.07 on the figure) and LEPTO 6.1, both of which are based on the Lund string fragmentation framework. The data shown in Figs. 5.4 and 5.5 are reasonably described by CDM, whereas the overall E_T predicted by LEPTO 6.1 is far too low. Unfortunately this version of LEPTO is very sensitive to the cut-off applied to avoid divergences in the matrix element — the boson-gluon-fusion (BGF) process, which is the dominant $\mathcal{O}(\alpha_S)$ graph at low Q^2 and x , creates two Lund strings as opposed to only one from the QCD

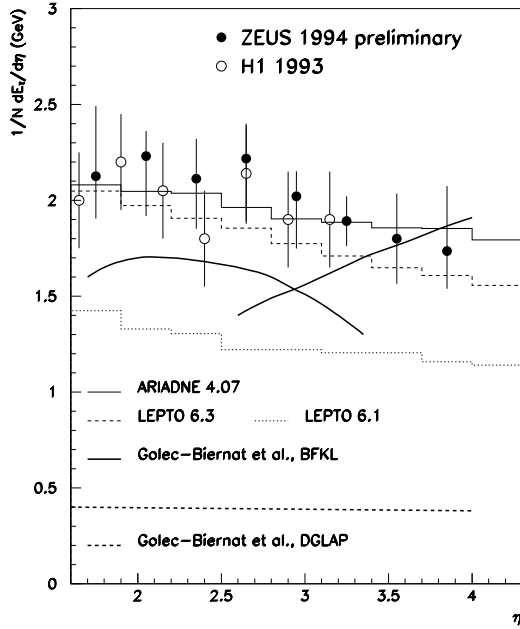


Figure 5.4. Mean transverse energy per unit rapidity in the forward region of the HERA lab. system.

Compton process or a $\mathcal{O}(\alpha_S^0)$ scattered quark. The effect of the presence of strings is an increased amount of E_T available in the hadronisation phase. A newer version of the program, LEPTO 6.3, reduced this dependence on the matrix element cut-off by treating the scattering off a sea quark in a manner similar to the 2 string scenario of the BGF case. Using this version of the generator allows a better description of the data, though there are still some problems in describing the x dependence in the lowest Q^2 region as shown in Figs. 5.4 and 5.5. However, the measurement seems to be rather sensitive to the non-perturbative hadronisation phase and can, in its present form, no longer be considered as a direct sensitive test of BFKL dynamics.

5.5. Deep inelastic events containing a forward jet

Another possible signature of the BFKL dynamics is the behaviour of deep inelastic (x, Q^2) events which contain a measured jet (x_j, k_{Tj}^2) in the kinematic regime where $k_{Tj}^2 \simeq Q^2$ (so as to neutralise the ordinary gluon radiation which would have arisen from GLAP evolution) and where the jet has longitudinal momentum fraction x_j as large as is experimental feasible ($x_j \sim 0.1$). The aim is to observe events with x/x_j as small as possible. According to BFKL dynamics the differential structure function has a leading small x/x_j behaviour of the form [111]

$$x_j \frac{\partial F_2}{\partial x_j \partial k_{Tj}^2} \sim \alpha_S(k_{Tj}^2) x_j \left[g + \frac{4}{9} (q + \bar{q}) \right] \left(\frac{x}{x_j} \right)^{-\lambda}$$

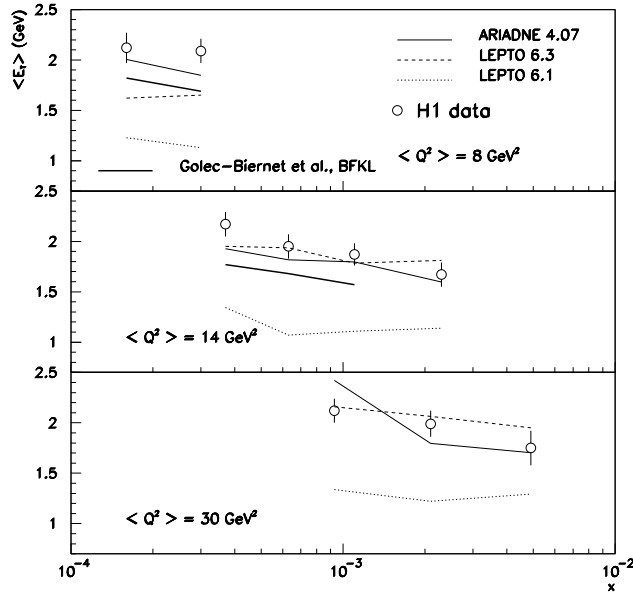


Figure 5.5. Transverse energy as a function of x for three different values of Q^2 . The transverse energy is measured in the CMS in the pseudorapidity range -0.5 to $+0.5$.

where the parton distributions are to be evaluated at (x_j, k_{Tj}^2) — where they are well known from global analyses. The idea is to see if the DIS + forward jet data show evidence of the $(x/x_j)^{-\lambda}$ behaviour. Jets are generally expected to be more robust against hadronisation effects than is the E_T flow.

We have studied DIS events at small x which have a jet with large x_j . A cone algorithm is used to find jets, requiring an E_T larger than 5 GeV in a cone of radius $R = \sqrt{\Delta\eta^2 + \Delta\phi^2} = 1.0$ in the space of pseudo-rapidity η and azimuthal angle ϕ in the HERA frame of reference. In order not to confuse the forward jet with the one at the top of the ladder the requirement $y > 0.1$ was imposed to ensure that the jet of the struck quark is well within the central region of the detector and is expected to have a jet angle larger than 60° . Experimentally a cone algorithm is used to find jets, requiring an E_T larger than 5 GeV in a cone of radius $R = \sqrt{\Delta\eta^2 + \Delta\phi^2} = 1.0$ in the space of pseudo-rapidity η and azimuthal angle ϕ in the HERA frame of reference. Jets are accepted as forward jets if $x_j > 0.025$, $0.5 < k_{Tj}^2/Q^2 < 4$, $6^\circ < \theta_j < 20^\circ$ and $k_{Tj} > 5$ GeV, where θ_j is the forward jet angle and k_{Tj} is the transverse momentum of the jet.

These selection criteria allow a study the cross section of forward jet production in the region $Q^2 \approx 20 \text{ GeV}^2$ and $2 \cdot 10^{-4} < x < 2 \cdot 10^{-3}$. Hence the ratio x_j/x is always larger than 10.

The resulting number of events observed with at least one forward jet in the kinematical region $160^\circ < \theta_e < 173^\circ$ and $E_e > 12$ GeV is given in Table 5.1 and compared to expectations of the MEPS and CDM models after detector simulation and corrected for background. The measured cross section for forward jets satisfying

x range	data events	MEPS events	CDM events	$\sigma(ep \rightarrow \text{jet}+X)$ (pb)
$2 \cdot 10^{-4} - 1 \cdot 10^{-3}$	271	141	282	$709 \pm 42 \pm 166$
$1 \cdot 10^{-3} - 2 \cdot 10^{-3}$	158	101	108	$475 \pm 39 \pm 110$

Table 5.1. Numbers of observed DIS events with a selected forward jet, corrected for radiative events faking this signature. These may be directly compared with the expectations from the Monte Carlo models. The measured cross section $ep \rightarrow \text{jet}+X$ for forward jets is also given. The errors reflect the statistical and systematic uncertainties.

the cuts given above is also presented in Table 5.1. It has been corrected for detector effects using the CDM. The ratio of the jet cross section for the low x to the high x bin is 1.49 ± 0.25 .

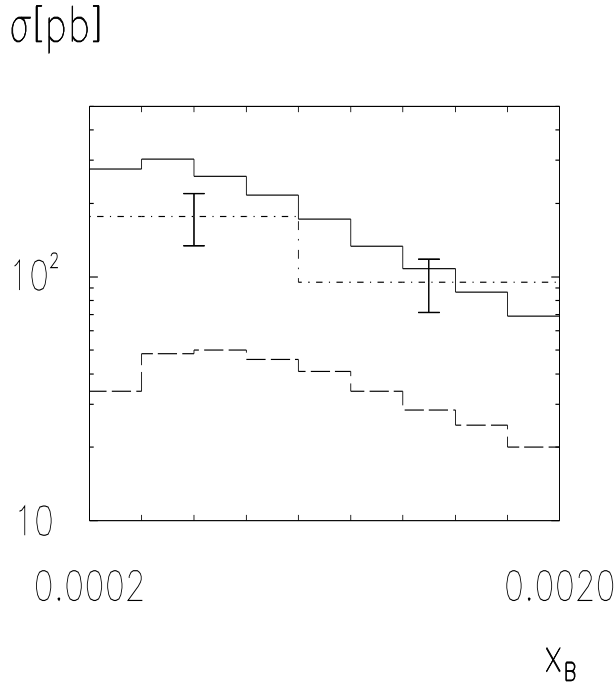


Figure 5.6. Comparison of the BKFL calculation and the approximate analytical calculation of the three-parton matrix elements, compared with the data of the H1 experiment.

In Fig. 5.6 the data are compared with a recent calculation [112]. The calculation (at the parton level) has exactly the same cuts as the measurement. The solid line is a BKFL calculation, while the dashed line is an approximate analytical three-parton matrix element calculation without the BKFL ladder. The results of H1 are compared with the calculations. The BKFL curve agrees well with the data, while the lower curve is in clear disagreement. Several corrections to this result should be considered,

as discussed in [112] (i.e. the calculation is at the parton level while the data are at the hadron level). Nevertheless the agreement with data is encouraging and such measurements should be explored further with larger statistics event samples as they have a large potential to reveal BFKL effects in the data.

A final general comment is in order. The smaller the value of x/x_j the larger is the BFKL effect and the more dominant is the leading $\log(1/x)$ formalism. As with all BFKL predictions, the reliability can only be quantified when the sub-leading corrections are known. Moreover by measuring properties of the final state we inevitably reduce the “reach” of HERA. For example in the present case we require x/x_j to be as small as possible, yet experimentally jet recognition demands $x_j \lesssim 0.1$, and so we lose an order of magnitude in “reaching small x ”.

6. Charm production

As we have seen above the gluon, the dominant parton at small x , has the least well determined distribution. Due to the theoretical uncertainties it is difficult to make unambiguous determinations of the gluon from the scaling violations that are observed in the HERA measurements of F_2 . The longitudinal structure function F_L gives, in principle, a much more direct determination of the gluon. In practice a sufficiently accurate measurement of F_L , which requires different beam energies, is exceedingly difficult. Here we note that F_2 itself contains an appreciable part which is directly sensitive to the gluon density, namely the contribution arising from charm production F_2^c .

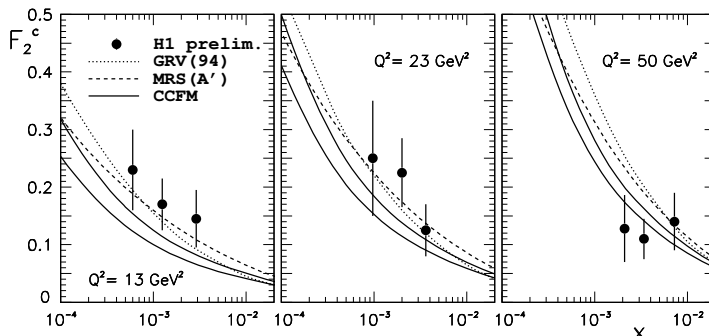


Figure 6.1. Predictions for F_2^c compared with preliminary H1 [113] data which became available after the Workshop. The curves show the predictions from MRS(A') partons [15] and from [114] using GRV partons (described in section 6.1), together with the CCFM prediction for $m_c = 1.4$ and 1.7 of ref. [86]. The figure is adapted from ref. [86].

At this Workshop both Vogt and Sutton presented predictions for F_2^c . The predictions are summarized in Fig. 6.1, which also contains preliminary measurements of F_2^c that became available after the Workshop [113]. The figure shows two calculations based on GLAP-evolved partons, (GRV, MRS), together with a prediction obtained using the unintegrated gluon distribution obtained by solving the CCFM equation (see section 4.4). All three calculations are quite different. MRS treat charm

as a parton and set $c(x, Q^2) = 0$ below some threshold $Q^2 < m^2$ and then use NLO GLAP evolution with $m_c = 0$. The calculation [114] using GRV partons treats charm as a heavy quark, not as a parton, and uses fixed-order (NLO) perturbation theory. We discuss this approach in detail below. Finally the CCFM predictions [86] are obtained from the unintegrated gluon distribution using the k_T -factorization theorem. They sum the LO $\log(1/x)$ contributions, but with the angular ordering constraints imposed.

6.1. Fixed-order prediction for F_2^c

At this Workshop, Riemersma presented the NLO QCD formalism for the \bar{c} contribution to F_2 . It is given by [115]

$$F_2^c(x, Q^2) = \frac{Q^2 \alpha_S(\mu^2)}{4\pi^2 m_c^2} \int_{ax}^1 \frac{dy}{y} yg(y, \mu^2) c_c^2 \left\{ c_{2,g}^{(0)} + 4\pi\alpha_S(\mu^2) \left[c_{2,g}^{(1)} + \bar{c}_{2,g}^{(1)} \ln \frac{\mu^2}{m_c^2} \right] \right\} \\ + \frac{Q^2 \alpha_S^2(\mu^2)}{\pi m_c^2} \sum_{i=1}^{2n_f} \int_{ax}^1 \frac{dy}{y} yq_i(y, \mu^2) \left[c_{2,i}^{(1)} + \bar{c}_{2,i}^{(1)} \ln \frac{\mu^2}{m_c^2} \right] \quad (6.1)$$

where here the sum is over the light quark flavours ($n_f = 3$). The ($\overline{\text{MS}}$) mass factorization scale μ has been put equal to the renormalization scale entering the strong coupling α_S . The lower limit of integration over the fractional initial-parton momentum y is given by $y_{\min} = ax = (1 + 4m_c^2/Q^2)x$, corresponding to the threshold $\hat{s} = 4m_c^2$ of the partonic center-of-mass (c.m.) energy squared. The coefficient functions c_2 can be expressed [115] in terms of the dimensionless variables

$$\xi = \frac{Q^2}{m_c^2}, \quad \eta = \frac{\hat{s}}{4m_c^2} - 1 = \frac{\xi}{4} \left(\frac{y}{x} - 1 \right) - 1. \quad (6.2)$$

In leading order, $\mathcal{O}(\alpha_S)$, F_2^c is directly sensitive only to the gluon density $g(y, \mu^2)$ via the well-known Bethe-Heitler process $\gamma^*g \rightarrow c\bar{c}$ [116]. A comparison of the various contributions to F_2^c in NLO shows that for the physically reasonable scales μ , $\mu \simeq 2m_c, \dots \sqrt{Q^2 + 4m_c^2}$ (see below), the quark contribution in (6.1) — which is not necessarily positive due to mass factorization — is very small, typically about 5% or less. Therefore F_2^c does represent a clean gluonic observable also in NLO.

Before considering the phenomenological consequences of (6.1), it is instructive to recall the η -dependence of the gluonic coefficient functions [115, 117]. They are displayed in Fig. 6.2 for two values of Q^2 typical for deep-inelastic small- x studies at HERA, $Q^2 = 10, 100 \text{ GeV}^2$. Here and in the following we take $m_c = 1.5 \text{ GeV}$. The comparison of the NLO coefficients $c^{(1)}$ and $\bar{c}^{(1)}$ with the Bethe-Heitler result $c^{(0)}$ reveals that potentially large corrections arise from regions where $c^{(0)}$ is small, namely from very small and very large partonic c.m. energies. These corrections are due to initial-state-gluon bremsstrahlung and the Coulomb singularity at small \hat{s} (small η), and due to the flavour excitation process at $\hat{s} \gg 4m_c^2$ ($\eta \gg 1$). The large logarithms $\ln[\hat{s}/(4m_c^2)]$ originating from flavour excitation have been resummed — at the expense of losing the full small- \hat{s} information of (6.1) — by introducing a charm parton density, leading to the so-called variable-flavour scheme [118]. The importance of these corrections in the HERA small- x regime considered here will be investigated below.

The first question to be addressed in order to judge the phenomenological usefulness of F_2^c as a gluon constraint is whether or not the available NLO expression

(6.1) is sufficient for obtaining results which are stable under variation of the (unphysical) mass factorization scale. It has been argued in [119] that one should use $\mu \simeq 2m_c$. This is motivated by the conjecture that μ is controlled by \hat{s} and the fact that the integrand in (6.1) is maximal close to the lower limit, $\hat{s} \simeq 4m_c^2$. The range of significant contributions in \hat{s} , however, broadens considerably with increasing Q^2 , as we shall see below, hence $\mu \simeq \sqrt{Q^2 + 4m_c^2}$, chosen in [115, 116], appears at least equally reasonable. Therefore, we will estimate the theoretical uncertainty of F_2^c in NLO by varying the scale between $\mu = m_c$ and $\mu = 2\sqrt{Q^2 + 4m_c^2}$. The corresponding results for F_2^c are shown in Fig. 6.3 for some fixed values of x and Q^2 , using the parton densities of GRV [14], which are appropriate here as they treat charm as a massive quark and not as a parton. At small- x , $x < 10^{-2}$, the scale variation amounts to at most $\pm 10\%$. Also displayed in Fig. 6.3 are the results for the three CTEQ2 parton

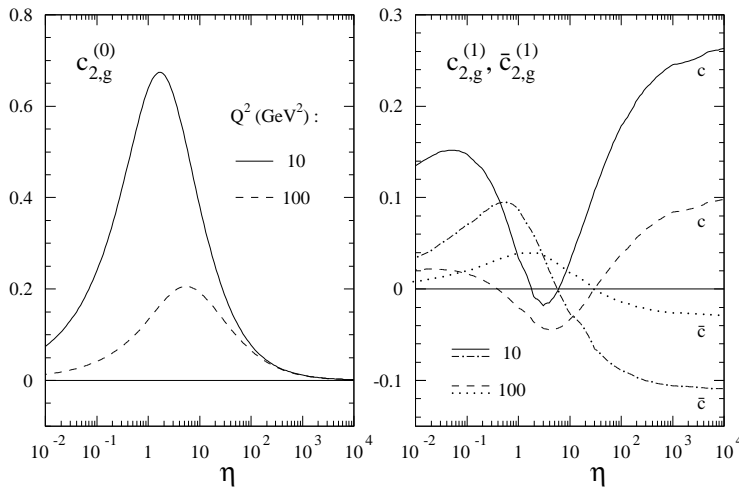


Figure 6.2. The η -dependence of the coefficient functions as parametrized in [116] for two values of Q^2 with $m_c = 1.5$ GeV. The scheme-dependent quantity $c_{2,g}^{(1)}$ is given in the $\overline{\text{MS}}$ scheme.

sets [120] at two selected values of x . Obviously the scale stability at small x does not significantly depend on the steepness of the gluon distribution. Consequently, the NLO results of [115, 116] seem to provide rather sound a theoretical foundation for a small- x gluon determination at HERA, despite the large total c.m. energy $s \gg 4m_c^2$ which might suggest a destabilizing importance of $\ln[\hat{s}/(4m_c^2)]$ terms. At large x , $x \approx 0.1$, on the other hand, the scale dependence of F_2^c is rather strong, especially at low Q^2 . Here, quantitatively reliable results require further theoretical input by resumming the large small- η threshold contributions mentioned above. However, F_2^c is small in this region.

The next issue we investigate is the locality (in the momentum fraction y) of the gluon determination via F_2^c . For this purpose, we replace the upper limit in (6.1) by a varying maximal gluon momentum $y_{\text{max}} < 1$. The contribution from initial-parton momenta smaller than y_{max} to $F_2^c(x, Q^2)$, denoted by $F_2^c(x, Q^2, y_{\text{max}})$, is presented in Fig. 6.4 for the GRV parton distributions [14]. At scales $\mu \approx \sqrt{Q^2 + 4m_c^2}$, about

80% of F_2^c originates in the region $y_{\min} = ax \leq y \lesssim 3y_{\min}$. Again the situation is very similar for the CTEQ2 parton densities [120]. Thus F_2^c allows for rather local a determination of $g(y, \mu^2 \approx \sqrt{Q^2 + 4m_c^2})$. The partonic c.m. energies in the region contributing 80% to the structure function F_2^c are given by $\eta \lesssim 5$ (20), corresponding to $\hat{s} \lesssim 60$ (180) GeV^2 , at $Q^2 = 10$ (100) GeV^2 , respectively. This implies that for the Q^2 values under consideration here, the plateau region of $c_{2,g}^{(1)}$ and $\bar{c}_{2,g}^{(1)}$ at large η (c.f. Fig. 6.2) does not play any important role. Resummation of large- η flavour excitation logarithms is thus neither necessary nor appropriate, especially if it implies additional approximations in the more important small- \hat{s} region [118]. A similar observation has already been made in [119] for $\mu \simeq 2m_c$ at low Q^2 . Note, however, that the latter scale choice leads to a considerably wider important range of \hat{s} at high Q^2 , somewhat in contrast to its motivation described above.

The expected x -dependence of F_2^c and its relative contribution to the total proton structure function F_2 are displayed in Fig. 6.5. F_2^c is large in the HERA small- x region (see Fig. 6.1). The absolute magnitude amounts to about 0.2...0.4, i.e. F_2^c is as large here as the total F_2 in the BCDMS/NMC fixed-target kinematical regime, making up up to a quarter of F_2 measured at HERA. This is in contrast to the bottom contribution F_2^b , which reaches at most 2...3%. The size of F_2^c renders a reliable (fully massive) treatment mandatory in any precise analysis of F_2 at small x . The sensitivity of F_2^c to the gluon density is illustrated by the difference of the CTEQ 2MF (flat $xg(x, \mu^2 = 2.6 \text{ GeV}^2)$ [120] and the GRV (steep gluon) [14] expectations. There is quite some discriminative power of F_2^c , especially close to the lower end of the Q^2 range considered here, $Q^2 \approx 10 \text{ GeV}^2$. Moreover, by measuring up to about 100 GeV^2 in Q^2 , the rapid growth of $yg(y \ll 1, \mu^2)$ predicted by the GLAP equations can be rather directly tested down to $y \simeq 10^{-3}$. A theoretical obstacle to an easy accurate gluon determination via the charm structure function is the dependence of F_2^c on the unknown precise value of the charm quark mass m_c . A 10% variation of m_c to 1.35 GeV and 1.65 GeV as also considered in Fig. 4 leads to a $\pm 15 \dots 25\%$ (5...10%) effect

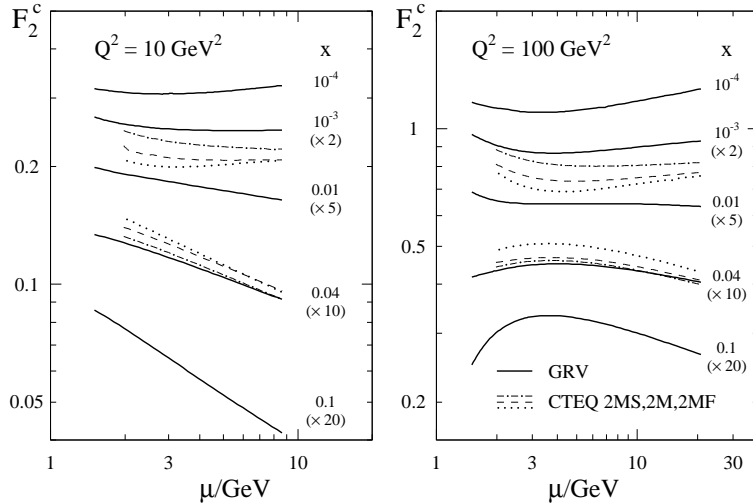


Figure 6.3. The dependence of F_2^c on the mass factorization scale μ in the region $m_c \leq \mu \leq 2(Q^2 + 4m_c^2)^{0.5}$ at selected values of x and Q^2 . The parton densities of GRV [14] (at all x) and CTEQ2 [120] (at $x = 10^{-3}, 0.04$) have been employed.

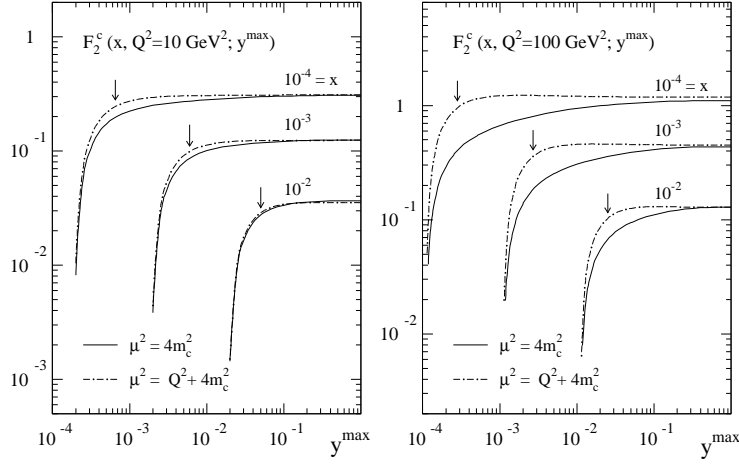


Figure 6.4. The contribution of the initial-parton momentum region $ax \leq y \leq y^{\max}$ to F_2^c at small- x for two choices of the scale μ , using the parton densities of [14]. The arrows indicate the values of y^{\max} at which 80% of the complete results are reached for $\mu = (Q^2 + 4m_c^2)^{0.5}$.

at $Q^2 = 10 (100) \text{ GeV}^2$, respectively, with respect to the central curves.

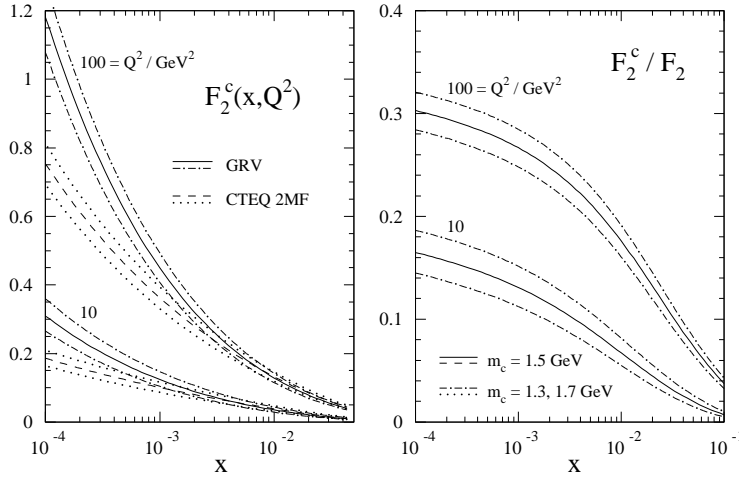


Figure 6.5. The x -dependence of F_2^c and F_2^c/F_2 at some fixed values of Q^2 , as expected from the GRV gluon density [14]. Also shown are F_2^c as obtained from the CTEQ 2MF parton set [120] and the charm mass dependence of the predictions. $\mu = (Q^2 + 4m_c^2)^{0.5}$ has been employed.

6.2. Outlook for F_2^c

The measurement of F_2^c at HERA should serve as a sensitive probe of the gluon at small x . In section 6.1 we have seen that the fixed-order QCD predictions are stable, with scale variations of less than $\pm 10\%$, and offer a rather local measurement of the gluon. Flavour excitation contributions from $\hat{s} \gg 4m_c^2$ become important only at scales Q^2 higher than those relevant for the small x observations at HERA.

Investigations of the effects of $\log(1/x)$ resummations have started (see Fig. 6.1 and also [79, 86]) but as yet the theoretical framework is much more incomplete than the fixed-order approach. Ultimately these effects may have to be incorporated in a detailed analysis of future precision data for F_2^c .

6.3. J/ψ production as a probe of the gluon

It has long been advocated that inelastic J/ψ photoproduction at HERA may serve as a measure of the gluon — see, for example, [121] or the review [122] which consider the process at leading-order accuracy. Recently the higher-order corrections to this process have been calculated [123, 124]. A detailed analysis of the spectra in the high energy range at HERA shows that the perturbative calculation is not well-behaved in the limit $p_T \rightarrow 0$, where p_T is the transverse momentum of the J/ψ . No reliable

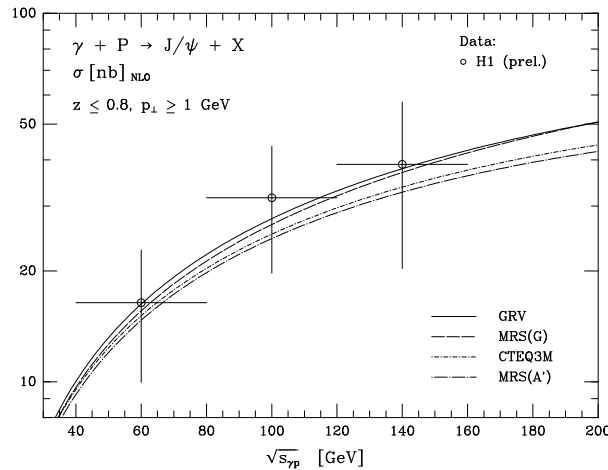


Figure 6.6. Total cross section for inelastic J/ψ photoproduction as a function of the photon-proton energy for different parametrizations of the parton distribution in the proton. Experimental data from [125]. The figure is from [124].

prediction can be made in this singular boundary region without resummation of large logarithmic corrections caused by multiple gluon emission. If the small p_T region is excluded from the analysis, the next-to-leading order result accounts for the energy dependence of the cross section and for the overall normalization, see Fig. 6.6 [124]. However, since the average momentum fraction of the partons is shifted to larger values when excluding the small- p_\perp region, the sensitivity of the prediction to the small- x behaviour of the gluon distribution is not very distinctive.

Diffractive J/ψ photoproduction appears to offer a more promising way to

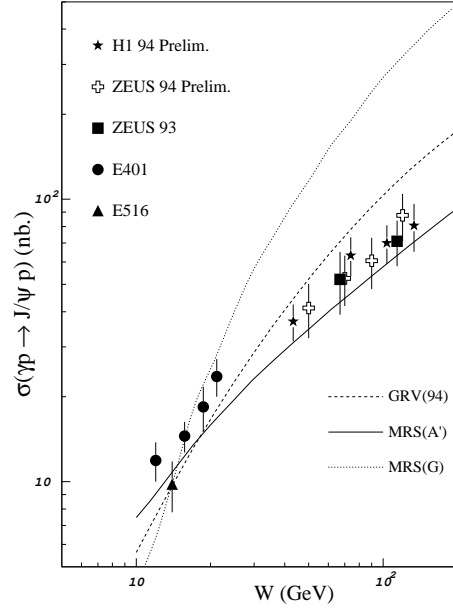


Figure 6.7. The measurements of the cross section for diffractive J/ψ photoproduction compared with the full perturbative QCD prediction obtained from the three latest sets of partons. The figure is taken from [128].

distinguish between the gluon distributions. Since this is essentially an elastic process the cross section is a measure of the square of the gluon density. To leading order the cross section is given by [126, 127]

$$\left. \frac{d\sigma}{dt} (\gamma^* p \rightarrow J/\psi p) \right|_0 = \frac{\Gamma_{ee} M_\psi^3 \pi^3}{48\alpha} \frac{\alpha_S(\bar{Q}^2)^2}{\bar{Q}^8} [xg(x, \bar{Q}^2)]^2 \quad (6.3)$$

with $\bar{Q}^2 = \frac{1}{4}M_\psi^2$ and $x = M_\psi^2/W^2$, where W is the γp c.m. energy. In a study which originated at the Workshop [128], corrections to this formula have been calculated and comparisons with HERA data made, see Fig. 6.7. It was emphasized that the W dependence, rather than the normalisation, was the more reliable discriminator between the gluons. The power of the method is evident from Fig. 6.7, which appears to favour the MRS(A') gluon.

7. Spin physics

Interest in spin phenomena in deep inelastic scattering revived in the eighties after the European Muon Collaboration discovered that the spin dependent structure function of the proton violates the Ellis-Jaffe sum rule and that the quarks probably carry only a small part of the total proton spin. The problem of the origin of the proton spin has led to an intense experimental and theoretical activity but in spite of that it has not yet been answered conclusively. Here we briefly review the status of the spin effects in deep inelastic scattering; experimental results and their theoretical interpretations.

Finally its future prospects will be outlined.

7.1. Cross section asymmetries and sum rules

The deep inelastic lepton-nucleon scattering cross section is the sum of a spin independent term $\bar{\sigma}$ and a term proportional to the lepton helicity h_l :

$$\sigma = \bar{\sigma} + \frac{1}{2}h_l\Delta\sigma. \quad (7.1)$$

Only longitudinally polarised leptons will be considered and the spin vector s_l is thus related to the lepton four momentum vector k . $\Delta\sigma$ gives only a small contribution to the total deep inelastic cross section. It depends on the two structure functions g_1 and g_2 and can be expressed as

$$\Delta\sigma = \cos\psi \Delta\sigma_{\parallel} + \sin\psi \cos\phi \Delta\sigma_{\perp}, \quad (7.2)$$

with

$$\begin{aligned} \frac{d^2\Delta\sigma_{\parallel}}{dx dQ^2} &= \frac{16\pi\alpha^2 y}{Q^4} \left[\left(1 - \frac{y}{2} - \frac{\gamma^2 y^2}{4}\right) g_1 - \frac{\gamma^2 y}{2} g_2 \right], \\ \frac{d^3\Delta\sigma_T}{dx dQ^2 d\phi} &= -\cos\phi \frac{8\alpha^2 y}{Q^4} \gamma \sqrt{1 - y - \frac{\gamma^2 y^2}{4}} \left(\frac{y}{2} g_1 + g_2 \right). \end{aligned} \quad (7.3)$$

In the above expressions, ψ denotes the angle between the lepton and the nucleon spin and ϕ the angle between the scattering plane and the spin plane; furthermore $\Delta\sigma_{\perp} = \Delta\sigma_T / \cos\phi$. $y = \nu/E$ and $\gamma = 2Mx/\sqrt{Q^2}$ are the usual kinematical factors.

In experimental measurements, two asymmetries can be defined:

$$A_{\parallel} = \frac{\Delta\sigma_{\parallel}}{2\bar{\sigma}} \quad \text{and} \quad A_{\perp} = \frac{\Delta\sigma_{\perp}}{2\bar{\sigma}}. \quad (7.4)$$

These asymmetries are directly related to the virtual photon asymmetries, A_1 and A_2 :

$$A_{\parallel} = D(A_1 + \eta A_2), \quad A_{\perp} = D(A_2 - \xi A_1), \quad (7.5)$$

where

$$A_1 = \frac{g_1 - \gamma^2 g_2}{F_1}, \quad A_2 = \gamma \frac{g_1 + g_2}{F_1}. \quad (7.6)$$

D , often called the depolarisation factor of the virtual photon, depends on y and the structure function $R = F_L/F_T$; factors η and ξ depend only on kinematic variables. A_1 and A_2 are often interpreted as virtual photon – nucleon asymmetries. They satisfy the bounds $|A_1| \leq 1$, $|A_2| \leq \sqrt{R}$.

Within the QPM the spin dependent structure function g_1 is given by

$$g_1(x) = \frac{1}{2} \sum_{i=1}^{n_f} e_i^2 [\Delta q_i(x) + \Delta \bar{q}_i(x)], \quad (7.7)$$

with $\Delta q_i(x) = q_i^+(x) - q_i^-(x)$, where q^{\pm} are the distribution functions of quarks with spin parallel (antiparallel) to the nucleon spin. Less obvious is the meaning of g_2 which contains a leading twist part, completely determined by g_1 and a higher twist

part, the meaning of which is subject to debate [129]. In QCD, g_1 evolves according to Altarelli–Parisi equations, similar to the unpolarised ones. Corresponding coefficient- and splitting functions have recently been calculated up to order α_S^2 [130], permitting the next-to-leading order QCD analysis of g_1 and thus a determination of the polarised parton distributions, $\Delta q_i(x, Q^2)$. Various groups have used the recent data to determine these distributions, taking into account the leading order QCD corrections†. A comparison of different parametrizations [132] shows that the polarised valence quark distributions $\Delta u_v(x, Q^2)$ and $\Delta d_v(x, Q^2)$ can be determined with some accuracy from the data, while the polarised sea quark and gluon distributions $\Delta \bar{q}(x, Q^2)$ and $\Delta g(x, Q^2)$ are only loosely constrained by the structure function measurements.

Contrary to g_1 and g_2 , definite theoretical predictions exist for the first moment of g_1 , $\Gamma_1 = \int_0^1 g_1(x) dx$, which measures the expectation value of the axial vector current between two nucleon states. Two sum rules exist for Γ_1 . The fundamental one was obtained by Bjorken [133] from the current algebra and isospin symmetry between the proton and the neutron:

$$\Gamma_1^p - \Gamma_1^n = \frac{1}{6} \left| \frac{g_A}{g_V} \right| = \frac{1}{6} (\Delta u - \Delta d) \quad (7.8)$$

where g_A and g_V are the axial and vector weak coupling constants in the neutron beta decay. The QCD corrections to this sum rule have been computed up to the order α_S^3 [134] and the $\mathcal{O}(\alpha_S^4)$ have been estimated [135].

Separate sum rules, obtained by Ellis and Jaffe [136], hold for the proton and the neutron:

$$\Gamma_1^{p(n)} = \pm \frac{1}{12} \left| \frac{g_A}{g_V} \right| + \frac{1}{36} a_8 + \frac{1}{9} \Delta \Sigma \quad (7.9)$$

Here $\Delta \Sigma = \Delta u + \Delta d + \Delta s$ is the flavour singlet axial coupling and Δq denote first moments of the spin dependent parton distributions in the proton, $\Delta q = \int_0^1 \Delta q_i(x) dx$; a_8 (and $|g_A/g_V|$) are related to the symmetric and antisymmetric weak flavour-SU(3) couplings in the baryon octet. If the flavour-SU(3) is exact then a_8 can be predicted from measurements of hyperon decays. There is however no prediction for $\Delta \Sigma$, except for $\Delta s=0$. In this case $\Delta \Sigma = a_8$, as was assumed in the original formulation by Ellis and Jaffe [136]. QCD corrections to these sum rules have been calculated up to the order α_S^2 [137] and the $\mathcal{O}(\alpha_S^3)$ have been estimated [138]. Due to the axial anomaly of the singlet axial vector current, $\Delta \Sigma$ is intrinsically Q^2 -dependent. Depending on the factorization scheme applied [139] this results either in a scale-dependence of the sea quark polarization or in an extra contribution to the Ellis–Jaffe sum rule, involving $\Delta g = \int_0^1 [g^+(x) - g^-(x)] dx$, the gluonic equivalent of the quark distribution moments. Both formulations are equivalent.

Higher twist effects in the Q^2 dependence of Γ_1 will not be considered here.

Evaluation of the Γ_1 requires knowledge of g_1 in the entire interval from 0 to 1. Measurements cover a limited kinematic range and thus extrapolations of g_1 to 0 and 1 are necessary. The latter is not critical since $g_1 \rightarrow 0$ at $x \rightarrow 1$ but the former is a considerable problem since g_1 increases as x decreases and its behaviour at low x is theoretically not understood, see sect.7.4. Therefore results on Γ_1 depend on the assumptions made in the $x \rightarrow 0$ extrapolation. Both SMC and SLAC experiments assume the Regge like behaviour of g_1 , i.e. that at $x \rightarrow 0$, g_1 behaves like x^α , $0 \leq \alpha \leq$

† Several analyses [131] incorporating NLO corrections [130] have appeared after this Workshop.

0.5. A value $\alpha=0$ was chosen and g_1 was fitted to the two data points at lowest x , allowing for variation of this behaviour within the Regge model. This approach might however be inconsistent with QCD which predicts a faster rise of g_1 at low x .

7.2. Experiments

New generation polarised electroproduction experiments are listed in table 7.1.

The experiment of the Spin Muon Collaboration (SMC) at CERN uses a naturally polarised muon beam and a cryogenic, solid state target. Experiments E142 – E155 at SLAC use an electron beam and liquid (solid) cryogenic targets. The HERMES experiment at DESY uses an electron beam from the HERA collider and internal gas targets. The scattered muon spectrometers in the SMC and SLAC experiments have been used (with little change) in DIS experiments preceding the polarised programme, contrary to the HERMES apparatus. Electron and muon measurements are complementary: the former offers very high beam intensities and thus statistics but its kinematic acceptance is limited to low values of Q^2 and moderate values of x , the latter extends to higher Q^2 and down to low values of x (an important aspect in the study of sum rules) but due to limited muon intensities the data taking time has to be long to ensure a satisfactory statistics.

Table 7.1. New generation experiments on polarised deep inelastic charged lepton – nucleon scattering. The last column shows references to the principal physics results obtained until now, (from [140]).

Experiment	Beam	Year	Beam energy (GeV)	Target	References
SMC	μ^+	1992–5	100,190	C ₄ D ₉ OD	[141, 142]
		1993	190	C ₄ H ₉ OH	[143, 144]
		1996	190	NH ₃	
E142	e^-	1992	19.4 –25.5	³ He	[145]
E143	e^-	1993	29.1	NH ₃ , ND ₃	[146, 147]
E154	e^-	1995	50	³ He	
E155	e^-	1996	50	NH ₃ , ND ₃	
HERMES	e^-	1995–	30–35	H, D, ³ He	

The lowest x in the results published by the SMC is about 10^{-3} and corresponds to Q^2 about 1 GeV². In the course of analysis are events having lower Q^2 and reaching x values of 10^{-4} . A special trigger has been set up recently to extend the measurements down to $x=10^{-5}$, at the expense of lowering Q^2 to 0.01 GeV². The upper limit of Q^2 in the SMC is about 100 GeV². The SLAC experiments' acceptance extends from x about 0.01 at $Q^2 = 1$ GeV² up $Q^2 \approx 10$ GeV² at $x \sim 0.7$. As in all fixed-target experiments, the low values of x in the SMC and SLAC are correlated with low Q^2 .

The cross section asymmetry measured in the polarised lepton – polarised nucleon experiments, A_{exp} , is related to the asymmetries defined in eq.(7.4) by $A_{exp} = f P_t P_b A$ where P_t, P_b denote the target and beam polarisations and f , the target dilution factor, accounts for the fact that only a fraction of nucleons is polarised. The beam polarisation at the SMC has been measured with a purpose-built polarimeter, using two independent methods: polarised μe scattering and an analysis of the energy spectrum of electrons coming from the muon decay. The result is $P_\mu = -0.790 \pm 0.025$

at 190 GeV beam energy. The target, subdivided into two cells polarised in opposite directions, was typically polarised up to 50% for the deuteron and 85% for the proton target. The target spin directions were reversed 5 times a day. Polarisation of the SLAC electron beam reached 86% in the E143 and was randomly reversed. Polarisation of the targets reached 80% for the proton and 25% for the deuteron one in E143. Systematic uncertainties in the SMC and SLAC experiments are similar.

7.3. Results of the measurements and spin structure of the nucleon

Cross section asymmetries A_1 and spin dependent structure functions g_1 have been measured for the proton and deuteron targets by the SMC, [141, 142, 143, 144] and by the E143, [146, 147]. Information on the neutron has been evaluated from the data on ^3He (E142, [145]) and from the data on the proton and deuteron (SMC, [141, 142]). All data sets are in a very good mutual agreement even if A_1 , extracted from data covering different Q^2 intervals, has been assumed to be Q^2 independent.

Results on g_1 for proton, deuteron and neutron are shown in Figs. 7.1, 7.2. Here $g_1^n = 2g_1^d/(1 - 1.5\omega_D) - g_1^p$ where $\omega_D \sim 0.05$ is the probability of the D-state of the deuteron. Conversion of A_1 to g_1 , which was made under an assumption that A_1 scales, needs only information on the structure function F_1 or, equivalently, F_2 and R (cf. eq.(7.6)). The NMC parametrisation of $F_2(x, Q^2)$ [64] and the SLAC parametrisation of $R(x, Q^2)$ [49] have been used by both SMC and SLAC.

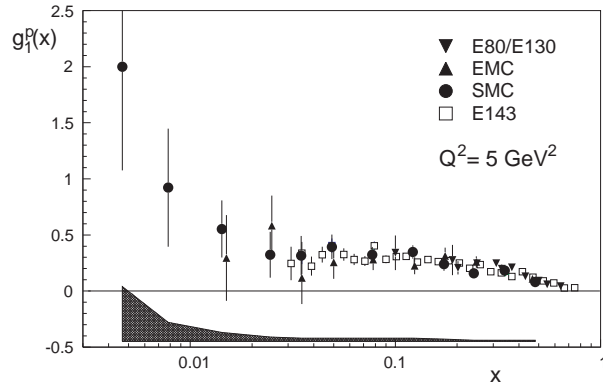


Figure 7.1. The spin dependent structure function $g_1(x)$ of the proton at $Q^2=5$ GeV^2 . the EMC data were reevaluated using the same F_2 and R parametrisations as for the SMC and E143 data. Error bars are statistical; the shaded area marks the SMC systematic errors. Figure taken from [140].

The behaviour of the g_1^p is different from that of g_1^d and g_1^n , especially at low x . This should be contrasted with the unpolarised case where a small difference between proton and neutron structure functions can be explained by nuclear shadowing in the deuteron. Measurements of the asymmetry, A_2 , for the proton [144] and the deuteron [148] showed that this function is significantly smaller than the bound \sqrt{R} and consistent with zero.

The Bjorken sum rule seems to be fulfilled by the above data at the 10% level: its value measured by the SMC at $Q^2 = 10 \text{ GeV}^2$ is $\Gamma_1^p - \Gamma_1^n = 0.199 \pm 0.038$, to be compared

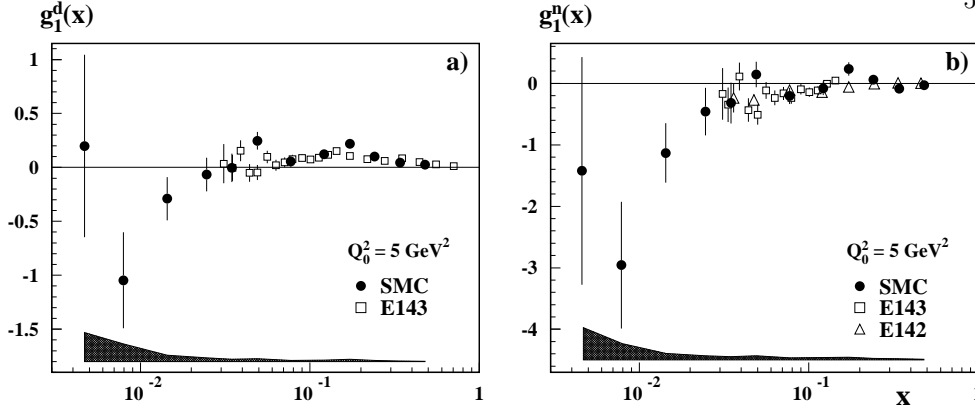


Figure 7.2. The spin dependent structure functions (a) $g_1^d(x)$ and (b) $g_1^n(x)$, as a function of x at $Q_0^2=5 \text{ GeV}^2$. error bars are statistical; the shaded area marks the SMC systematic errors. Figure taken from [142].

with the QCD prediction (four flavours, corrections up to α_s^3): 0.187 ± 0.003 . The Ellis-Jaffe sum rule is not confirmed by the data, the pattern of disagreement being similar in the proton and deuteron results. At $Q^2 = 5 \text{ GeV}^2$, the combined data of the EMC, SMC and SLAC give for Γ_1^p , Γ_1^d and Γ_1^n respectively: 0.125 ± 0.009 , 0.041 ± 0.005 and -0.037 ± 0.008 as compared to the predicted 0.167 ± 0.005 , 0.070 ± 0.004 and -0.015 ± 0.005 . A most straightforward explanation of this violation may be a non-zero polarisation of the strange sea. Results of the new SMC proton data analysis, with extended kinematic coverage and a NLO QCD analysis to evolve the measured $g_1(x, Q^2)$ to a common value of Q^2 , confirm all the above conclusions.

The nucleon spin, $S_z = \frac{1}{2}$, can be decomposed as follows

$$S_z = \frac{1}{2} \Delta \Sigma + \Delta g + L_z \quad (7.10)$$

where L_z is angular momentum due to the partons. All the data sets (except perhaps E142), evaluated with a consistent treatment of the QCD corrections at a common $Q^2=5 \text{ GeV}^2$ and under the assumption that the flavour SU(3) is exact, show that the total quark contribution to the nucleon spin is small, $\Delta \Sigma \sim 0.2$, and that the strange sea is indeed polarised: $\Delta s \sim -0.1$. SU(3)-breaking can decrease Δs but leaves $\Delta \Sigma$ unchanged. Choosing a factorization scheme in which the quarks polarisation is scale independent, a Q^2 dependent gluonic contribution appears in the Ellis-Jaffe sum rule as a result of the anomalous dimension of the singlet axial vector current [139]. Then the Ellis-Jaffe assumption of $\Delta s=0$ implies that at $Q^2=5 \text{ GeV}^2$, $\Delta g \sim 3$ is needed to restore the sum rule.

Finally we note the first measurements of the semi-inclusive spin asymmetries for positively and negatively charged hadrons in the polarised muon-proton and muon-deuteron scattering in the SMC experiment [149]. The x dependence of the spin distributions for the up and down valence quarks and for the non-strange sea quarks has been determined. The moments of the quark spin distributions were obtained to be: $\Delta u_v = 1.01 \pm 0.24$, $\Delta d_v = -0.57 \pm 0.25$; moments for the non-strange sea quarks are consistent with zero over the whole measured range of x .

7.4. Theory predictions for g_1 at small x

Observation of a difference between the proton and deuteron spin structure functions $g_1^{p,d}(x, Q^2)$ at small x , Figs. 7.1, 7.2, indicates a sizeable *non-singlet* contribution to g_1 in this region. The dominant behaviour of $g_1^{n.s.}$ can be estimated from a resummation of the leading QCD corrections. The conventional Altarelli-Parisi approach only resums terms of the form $(\alpha_S \ln Q^2 \ln(1/x))^k$ and yields

$$g_1^{n.s.}(x, Q^2) \sim \exp\left(\sqrt{\frac{2\alpha_S C_F}{\pi} \ln \frac{Q^2}{\mu^2} \ln \frac{1}{x}}\right). \quad (7.11)$$

Terms proportional to $(\alpha_S \ln^2(1/x))^k$, which arise due to the presence of two fermions in the t -channel [150] are, although more singular at small x , not included.

Ryskin outlined a calculation of the small x behaviour of $g_1^{n.s.}$, which resums these contributions [151]. This calculation not only includes the enlarged (compared to the Altarelli-Parisi approach) phase space of ladder diagrams which leads to the double logarithmic contributions, but also substantially differs from similar resummations performed for unpolarised structure functions in that both ladder and non-ladder diagrams contribute to the most singular part of the amplitude. Using the fact that the non-ladder gluon has to be softer than all gluons within the ladder, these non-ladder contributions can be resummed. This procedure results in a nonlinear infrared evolution equation [152] for the quark amplitudes of odd signature, which mixes color-singlet and color-octet quark amplitudes. By means of a Mellin transformation, this equation can be solved, yielding

$$g_1^{n.s.} \sim x^{-\omega_{n.s.}^{(-)}} \quad \text{with } \omega_{n.s.}^{(-)} \simeq 1.04 \sqrt{2\alpha_S C_F/\pi} \simeq 0.4 \quad (\text{for } \alpha_S = 0.18). \quad (7.12)$$

The non-ladder (bremsstrahlung) contributions give a relatively small contribution (4%) to $\omega_{n.s.}^{(-)}$; if only ladder diagrams are retained then $\omega_{n.s.}^{(-)} = \omega_{n.s.}^{(+)} = \sqrt{2\alpha_S C_F/\pi}$ for fixed coupling. When running coupling effects are included in the double logarithmic resummation generated by the ladder diagrams then the effective slope is reduced to 0.2 - 0.3 [153].

First preliminary results of a similar calculation for the singlet contribution to $g_1(x)$ at small x were presented [154], indicating that

$$g_1^s \sim x^{-\omega_s^{(-)}} \quad \text{with } \omega_s^{(-)} \simeq 3 \omega_{n.s.}^{(-)} > 1 \quad (\text{for } \alpha_S > 0.12). \quad (7.13)$$

As the above result contradicts conventional Regge-type extrapolations of $g_1^{n.s.}$ in the Ellis-Jaffe sum rule, it shows the need for extending the measurements of $g_1(x, Q^2)$ down to the lowest possible values of x .

7.5. Prospects for the future

Understanding of the polarised structure functions has improved dramatically in the recent years, thanks to the EMC, SMC and SLAC measurements. Several questions however remained unanswered. Among them is the low x behaviour of g_1 , its Q^2 evolution, the gluon polarisation and flavour decomposition of polarised parton distribution. The HERMES experiment, recently starting at HERA, using a polarised electron beam and a polarised internal gas target will especially address the last question from a presently unique reconstruction of the hadronic final state. To answer

the remaining questions a new generation of experiments, e.g. at the HERA *collider*, is needed. Prospects of spin physics at HERA were discussed at a workshop at DESY-Zeuthen in August 1995. A polarised deep inelastic programme at HERA could allow measurements over an extended kinematic range, including low x and high Q^2 . Polarisation of the proton beam is technically much more complicated than polarisation of the electron beam, as the proton beam does not polarise naturally [155]. Construction of the polarised proton beams of energy up to 250 GeV in the RHIC collider rings has already been approved, a helpful step for HERA. Various suggestions for dedicated measurements of $\Delta g(x, Q^2)$, including the HMC/CHEOPS project at CERN, were also discussed at the Zeuthen workshop [156].

8. Conclusions

We believe that this report gives a fair summary of our present understanding of the structure of the proton, as it is seen in deep-inelastic lepton-proton scattering. Much — but not all — of the recent experimental information comes from HERA. We have summarized the HERA and fixed-target data in the first part of this Report.

The most puzzling phenomenon continues to be the rise of F_2 at small x , which seems to persist even at low values Q^2 , and its connection with the soft Pomeron seen in photoproduction at $Q^2 = 0$. So far there is no real problem in describing the inelastic data within the GLAP evolution scheme, i.e. it is possible to find starting distributions for quarks and gluons which evolve according to the (next-to-leading) QCD evolution equations and successfully describe the data. This alone, however, does not *explain* the observed rise: either one has to ascribe the origin of the rise to the input (gluon) distribution (the BFKL scenario), or one has to allow a rather large Q^2 range of the GLAP evolution. In the latter case, the GLAP evolution by itself leads to a rise at small x . But in order to accommodate the observed rise at low Q^2 the QCD evolution has to start at an even lower scale where - on rather general grounds - one would have been hesitant to use a leading-twist perturbative QCD framework. A further ambiguity is that, as yet, the “BFKL scenario” is based only on the resummation of leading $\log(1/x)$ terms. A quantitative description needs the computation of sub-leading effects.

The discussions of the Working Group, as described in this summary, reflect the agreement among the participants that we need a thorough understanding of the validity of GLAP and BFKL descriptions (and a description which unifies both) in the low- x and low- Q^2 region, as well as the interpolation between deep inelastic scattering and photoproduction, before a deeper understanding of the interface between perturbative and non-perturbative physics can be reached. It seems clear that to gain further insight we must study more than just the fully inclusive total cross section as measured by F_2 , i.e. we need to look more closely into the final state of deep-inelastic scattering.

The discussion of the spin structure of the proton also seems to be developing in the small- x direction, somewhat analogous to the unpolarized case. Namely, the low- x data points for both the proton and the neutron spin structure functions g_1 indicate the possibility of a rise at small x . At the same time QCD calculations, based on leading and next-to-leading order Altarelli-Parisi splitting functions or, more recently, using the double-logarithmic approximation, predict a strong rise of g_1 at small x . So there is little doubt that small- x physics is becoming a field of particular interest also in the proton spin community.

Acknowledgements

We thank all those who participated in the Proton Structure Working Group. In particular we thank the people who gave talks to the Group, including Johannes Blumlein, Tim Carroll, Stefano Catani, John Dainton, Sandy Donnachie, Leonid Frankfurt, Mark Gibbs, Tim Greenshaw, Franseco Hautmann, Rob Henderson, Indumathi, Dave Kant, Valeri Khoze, Jan Kwieciński, Genya Levin, Steve Riemersma, Misha Ryskin, Bill Seligman, Tara Shah, Torbjorn Sjöstrand and Peter Sutton, besides the authors. We especially thank Keith Ellis who, at very short notice, presented the summary talk for our group, and Mike Whalley, as well as Robin Devenish, for such excellent organisation before, during and after the Workshop. We are grateful to Michael Krämer for useful information. We also thank Sharon Fairless and Rachel Lumpkin for their invaluable help in processing this article and PPARC for financial support.

References

- [1] A. De Roeck, J. Phys. **G19** (1993) 1549.
- [2] BFKL: E.A. Kuraev, L.N. Lipatov and V.S. Fadin, Phys. Lett. **B60** (1975) 50; Sov. Phys. JETP **44** (1976) 443; Sov. Phys. JETP **45** (1977) 199.
Ya. Ya. Balitsky and L.N. Lipatov, Sov. J. Nucl. Phys. **28** (1978) 822.
- [3] R.C.E. Devenish, J. Phys. **G19** (1993) 1425.
- [4] GLAP: V.N. Gribov and L.N. Lipatov, Sov. J. Nucl. Phys. **15** (1972) 438;
G. Altarelli and G. Parisi, Nucl. Phys. **B126** (1977) 298;
Yu. L. Dokshitzer, Sov. Phys. JETP **46** (1977) 641.
- [5] M. Lancaster, these proceedings.
- [6] H1 Collaboration: S. Aid *et al* DESY preprint, 96-039.
- [7] ZEUS Collaboration: M. Derrick *et al* DESY preprint 95-221 (1995).
- [8] G. Altarelli and G. Martinelli, Phys. Lett. **B76** (1978) 89.
- [9] NMC: M. Arneodo *et al* Phys. Lett. **B364** (1995) 107.
- [10] BCDMS Collaboration: A. C. Benvenuti *et al* Phys. Lett. **B223** (1989) 485;
ibid **B237** (1990) 592.
- [11] S. Bentvelsen, P. Kooijman and J. Engelen, Proc. of the Workshop *Physics at HERA*, ed. W. Buchmüller and G. Ingelman, Hamburg 23. (1992)
K.C. Hoeger, Proceedings of the Workshop *Physics at HERA*, ed. W. Buchmüller and G. Ingelman, Hamburg 43 (1992).
- [12] H1 Collaboration: T. Ahmed *et al* Nucl. Phys. **B439** (1995) 471.
- [13] U. Bassler and G. Bernardi, DESY preprint 94-231 (1994), submitted to Nucl. Inst. and Meth.
- [14] M. Glück, E. Reya and A. Vogt, Z. Phys **C67** (1995) 433.
- [15] A.D. Martin, R.G. Roberts and W.J. Stirling, Phys. Lett. **B354** (1995) 155.
- [16] CTEQ Collaboration: H.L. Lai *et al* Phys. Rev. **D51** (1995) 4763.
- [17] A. Donnachie and P.V. Landshoff, Z. Phys. **C61** (1994) 139.
- [18] A. Capella *et al* Phys. Lett. **B337** (1994) 358. For this calculation the intercept $1 + \delta$ was taken with $\delta = 0.25$ and no QCD evolution was used in the region shown.
- [19] F. Eisele, Proc. of Int. Europhysics Conf. on HE Physics, Brussels, 1995. DESY preprint 95-229.
- [20] A. Levy *et al* DESY preprint 95-204.
- [21] L.W. Whitlow *et al* Phys. Lett. **B282** (1992) 475.
- [22] NA28 Collaboration: M. Arneodo *et al* Nucl. Phys. **B333** (1990) 1.
- [23] J. Kwieciński and B. Badełek, Z. Phys. **C43** (1989) 251;
B. Badełek and J. Kwieciński, Phys. Lett. **B295** (1992) 263.
- [24] E665 Collaboration: A. V. Kotwal *et al* preprint FERMILAB-CONF-95-46 and Proc. of the XXX Rencontre de Moriond, *QCD and High Energy Hadronic Interactions*, March 1995, Les Arcs, France; A.V. Kotwal, Ph.D. Thesis, Harvard University, May 1995.
- [25] A.D. Martin, W.J. Stirling and R.G. Roberts, Phys. Lett. **B306** (1993) 145;
A.D. Martin, W.J. Stirling and R.G. Roberts, Phys. Rev. **D47** (1993) 867.
- [26] E665 Collaboration: M.R. Adams *et al* Phys. Rev. Lett. **75** (1995) 1466.
- [27] B. Badełek and J. Kwieciński, Phys. Rev. **D50** (1994) R4;

- [28] W. Melnitchouk and A.W. Thomas, Phys. Rev. **D47** (1993) 3783; Phys. Lett. **B317** (1993) 437;
V. Barone *et al* Phys. Lett. **B321** (1994) 137.
- [29] V.R. Zoller, Phys. Lett. **B279** (1992) 145; Z. Phys. **C54** (1992) 425.
- [30] NMC: A. Witzmann, Proc. of Int. Europhysics Conf. on HE Physics, Brussels, 1995.
- [31] NMC: P. Amaudruz *et al* Nucl. Phys. **B441** (1995) 3.
- [32] NMC: P. Amaudruz *et al* Nucl. Phys. **B441** (1995) 12.
- [33] E139 Collaboration: R.G. Arnold *et al* Phys. Rev. Lett. **52** (1984) 727.
- [34] E665 Collaboration: M.R. Adams *et al* Z. Phys. **C67** (1995) 403.
- [35] NMC: A. Mücklich, Proc. of the Workshop on the Deep Inelastic Scattering and QCD, Paris, 1995, eds J.-F. Laporte and Y. Sirois, p. 489.
- [36] E665 Collaboration: T. Carroll, these proceedings.
- [37] H1 Collaboration: S. Aid *et al* Phys. Lett. **B354** (1995) 494.
- [38] ZEUS Collaboration: M. Derrick *et al* Phys. Lett. **B345** (1995) 576. **B354** (1995) 155.
- [39] NMC: M. Arneodo *et al* Phys. Lett. **B309** (1993) 222.
- [40] M. Virchaux and A. Milsztajn, Phys. Lett. **B274** (1992) 221.
- [41] G. Thompson, these proceedings
- [42] H1 Collaboration: S. Aid *et al* Nucl. Phys. **B449** (1995) 3.
- [43] Report of the Diffractive group, these proceedings
- [44] A. Levy, these proceedings.
- [45] NMC: P. Amaudruz *et al* Phys. Lett. **B294** (1992) 120.
- [46] NMC: T. Granier, Proc. of the XXIX Rencontre de Moriond, *QCD and High Energy Interactions*, March 1994, Méribel, France.
- [47] NMC: A. Dyring, Ph.D. thesis, Uppsala University (1995).
- [48] CCFR Collaboration: U.K. Yang, these proceedings.
- [49] L.W. Whitlow *et al* Phys. Lett. **B250** (1990) 193.
- [50] B. Badelek, J. Kwieciński and A. Staśto, Durham preprint DTP/96/16.
- [51] S.A. Larin and J.A.M. Vermaseren, Phys. Lett. **B259** (1991) 345.
- [52] CCFR Collaboration: D.A. Harris *et al* Proc. of Int. Europhysics Conf. on HE Physics, Brussels, 1995. EPS-0043.
- [53] NMC: M. Arneodo *et al* Phys. Rev. **D50** (1994) R1.
- [54] NA51 Collaboration: A. Baldit *et al* Phys. Lett. **B332** (1994) 244.
- [55] NMC: A. Brüll, Proc. of Int. Europhysics Conf. on HE Physics, Brussels, 1995.
- [56] B. Badelek and J. Kwieciński, Rev. Mod. Phys. (in print).
- [57] B. Badelek *et al* Rev. Mod. Phys. **64** (1992) 927.
- [58] F.W. Brasse *et al* Nucl. Phys. **B110** (1976) 413.
- [59] CHIO Collaboration: Gordon *et al* Phys. Rev. **D20** (1979) 2645.
- [60] H. Abramowicz *et al* Phys. Lett. **B269** (1991) 465.
- [61] NMC: P. Amaudruz *et al* Nucl. Phys. **B371** (1992) 3.
- [62] G.A. Schuler and T. Sjöstrand, Nucl. Phys. **B407** (1993) 425.
- [63] A.D. Martin, W.J. Stirling and R.G. Roberts, Phys. Rev. **D51** (1995) 4756.
- [64] NMC: P. Amaudruz *et al* Phys. Lett. **B295** (1992) 159 and preprint CERN-PPE/92-124; Erratum Oct. 26th, 1992; Erratum April 19th, 1993; NMC: M. Arneodo *et al* Phys. Lett. **B364** (1995) 107.
- [65] NMC: A. Dyring, Proc. of the XXIX Rencontre de Moriond, *QCD and High Energy Hadronic Interactions*, March 1994, Méribel, France, edited by J. Trân Thanh Vân (Editions Frontières).
- [66] E665 Collaboration: M.R. Adams *et al* Phys. Lett. **B309** (1993) 477.
- [67] E665 Collaboration: M.R. Adams *et al* Phys. Rev. Lett. **68** (1992) 3266.
- [68] J. Kwieciński, these proceedings.
- [69] A. Levy, these proceedings.
- [70] R.G. Roberts, these proceedings.
- [71] A. DeRujula, S.L. Glashow, H.D. Politzer, S.B. Treiman, F. Wilczek, A. Zee, Phys. Rev. **D10** (1974) 1649.
- [72] R.D. Ball and S. Forte, Phys. Lett. **B335** (1994) 77; Phys. Lett. **B336** (1994) 77;
J.R. Forshaw and R.G. Roberts, Phys. Lett. **B351** (1995) 308.
- [73] H1 Collaboration: S. Aid *et al* Phys. Lett. **B354** (1995) 494.
- [74] T. Jaroszewicz, Phys. Lett. **B116** (1982) 291.
- [75] S. Catani and F. Hautmann, Phys. Lett. **B315** (1993) 157.
- [76] S. Catani and F. Hautmann, Nucl. Phys. **B427** (1994) 475;
J. Kwieciński and A.D. Martin, Phys. Lett. **B353** (1995) 123;

- M. Ciafaloni, Phys. Lett. **B356** (1995) 74.
- [77] V.S. Fadin and L.N. Lipatov, DESY preprint 96-020.
- [78] R.K. Ellis, Z. Kunszt and E.M. Levin, Nucl. Phys. **B420** (1994) 517;
R.K. Ellis, F. Hautmann and B.R. Webber, Phys. Lett. **B348** (1995) 582;
R.D. Ball and S. Forte, Phys. Lett. **B351** (1995) 513;
J.R. Forshaw, R.G. Roberts and R.S. Thorne, Phys. Lett. **B356** (1995) 79.
- [79] A.J. Askew, J. Kwieciński, A.D. Martin and P.J. Sutton, Phys. Rev. **D47** (1993) 3775; **D49** (1994) 4402.
- [80] S. Catani, M. Ciafaloni and F. Hautmann, Phys. Lett. **B242** (1990) 97; Nucl. Phys. **B366** (1991) 657.
- [81] J.C. Collins and R.K. Ellis, Phys. Lett. **B360** (1991) 3.
- [82] E.M. Levin, M.G. Ryskin and A.G. Shuvaev, Sov. J. Nucl. Phys. **53** (1991) 657.
- [83] J. Kwieciński, A.D. Martin and P.J. Sutton, Z. Phys. **C** (in press).
- [84] M. Ciafaloni, Nucl. Phys. **B296** (1988) 49;
S. Catani, F. Fiorani and G. Marchesini, Phys. Lett. **B234** (1990) 339; Nucl. Phys. **B336** (1990) 18.
- [85] J. Kwieciński, A.D. Martin and P.J. Sutton, Phys. Rev. **D52** (1995) 1445.
- [86] J. Kwieciński, A.D. Martin and P.J. Sutton, Durham preprint DTP/95/94, Phys. Rev. (in press).
- [87] H1 Collaboration: G. Raedel, Proc. of the Workshop on the Deep Inelastic Scattering and QCD, Paris, 1995, eds J.-F. Laporte and Y. Sirois, p. 223;
ZEUS Collaboration: M. Lancaster, Proc. of the Workshop on the Deep Inelastic Scattering and QCD, Paris, 1995, eds J.-F. Laporte and Y. Sirois, p. 229.
- [88] L.N. Gribov, E.M. Levin, M.G. Ryskin, Phys. Rep. **100** (1982) 1.
- [89] K. Golec-Biernat, M.W. Krasny and S. Riess, Phys. Lett. **B337** (1994) 367.
- [90] J. Bartels and M.G. Ryskin, Z. Phys. **C60** (1993) 751.
- [91] E.M. Levin, M.G. Ryskin and A.G. Shuvaev, Nucl. Phys. **B387** (1992) 589.
- [92] A.P. Bukhvostov, G.V. Frolov, L.N. Lipatov, E.A. Kuraev, Nucl. Phys. **B258** (1985) 601.
- [93] J. Bartels, Phys. Lett. **B298** (1993) 204.
- [94] R.P. Feynman, 'Photon-Hadron Interactions' (Benjamin, New York, 1972).
- [95] Yu. L. Dokshitzer *et al* Rev. Mod. Phys. **60** (1988) 373.
- [96] ZEUS Collaboration: M. Derrick *et al* Z. Phys. **C67** (1995) 93.
- [97] H1 Collaboration: S. Aid *et al* Nucl. Phys. **B445** (1995) 3.
- [98] HRS Collaboration: M. Derrick *et al* Phys. Rev. **D34** (1986) 3304;
MARK 1 Collaboration: J.L. Siegrist *et al* Phys. Rev. **D26** (1986) 969;
OPAL Collaboration: P.D. Acton *et al* Z. Phys. **C53** (1992) 539;
PLUTO Collaboration: Ch. Berger *et al* Phys. Lett. **B95** (1980) 313;
TASSO Collaboration: W. Braunschweig *et al* Z. Phys. **C45** (1989) 193.
- [99] M. Derrick *et al* Phys. Lett. **B91** (1980) 470.
- [100] ZEUS Collaboration: M. Derrick *et al* Z. Phys. **C68** (1995) 29.
- [101] H1 Collaboration: Proc. of Int. Europhysics Conf. on HE Physics, Brussels, 1995. Ref. 0479.
- [102] G. Ingelman, Proc. of the Workshop on Physics at HERA, Hamburg 1991, eds. W. Buchmüller and G. Ingelman, vol. 3, p. 1366.
- [103] L. Lönnblad, Comp. Phys. Comm. **71** (1992) 15.
- [104] T. Sjöstrand, talk presented to the Workshop.
- [105] M. Gibbs, A. Ringwald and F. Schrempp, Proc. of the Workshop on the Deep Inelastic Scattering and QCD, Paris, 1995, eds. J.-F. Laporte and Y. Sirois, p. 341.
- [106] M. Gibbs, talk presented to the Workshop.
- [107] L. Lönnblad, Z. Phys. **C65** (1995) 285;
A.H. Mueller, Nucl. Phys. **B415** (1994) 373;
L. Lönnblad, Proc. of PHOTON'95, Sheffield, 1995, eds. D.J. Miller, S.L. Cartwright and V.A. Khoze, p. 443.
- [108] K. Golec-Biernat, J. Kwieciński, A.D. Martin and P.J. Sutton, Phys.Lett. **B335** (1994) 220; Phys. Rev. **D50** (1994) 217.
- [109] H1 Collaboration: S. Aid *et al* Phys.Lett. **B356** (1995) 118.
- [110] ZEUS Collaboration: Proc. of Int. Europhysics Conf. on HE Physics, Brussels, 1995. Ref. 0391.
- [111] A.H. Mueller, Nucl. Phys. B (Proc. Suppl.) **18C** (1990) 125; J. Phys. **G17** (1991) 1443;
J. Kwieciński, A.D. Martin, P.J. Sutton, Phys. Rev. **D46** (1992) 921; Phys. Lett. **B287** (1992) 254; Nucl. Phys. B (Proc. Suppl.) **29A** (1992) 67.
J. Bartels, A. De Roeck, M. Loewe, Z. Phys. **C54** (1992) 635; Nucl. Phys. B (Proc. Suppl.) **29A** (1992) 61;

- W.K. Tang, Phys. Lett. **B278** (1992) 363.
- [112] J. Bartels *et al* DESY preprint 96-036.
- [113] H1 Collaboration: A. De Roeck, Proc. of Krakow Epiphany Conf., Jan. 1996, to be published in Acta Phys. Polon.
- [114] A. Vogt, DESY preprint 96-012, hep-ph/9601352.
- [115] E. Laenen, S. Riemersma, J. Smith and W.L. van Neerven, Nucl. Phys. **B392** (1993) 162.
- [116] S. Riemersma, J. Smith and W.L. van Neerven, Phys. Lett. **B347** (1995) 143.
- [117] E. Witten, Nucl. Phys. **B104** (1976) 445;
M. Glück and E. Reya, Phys. Lett. **83B** (1979) 98.
- [118] M.A.G. Aivazis, F.I. Olness and W.-K. Tung, Phys. Rev. **D50** (1994) 3085;
M.A.G. Aivazis, J. Collins, F.I. Olness and W.-K. Tung, Phys. Rev. **D50** (1994) 3102;
F.I. Olness and S.T. Riemersma, Phys. Rev. **D51** (1995) 4746.
- [119] M. Glück, E. Reya and M. Stratmann, Nucl. Phys. **B422** (1994) 37.
- [120] CTEQ Collaboration: J. Botts *et al* Phys. Lett. **B304** (1993) 159.
- [121] A.D. Martin, C.-K. Ng and W.J. Stirling, Phys. Lett. **B191** (1987) 200.
- [122] H. Jung, G.A. Schuler and J. Terrón, Int. J. Mod. Phys. **A7** (1992) 7955.
- [123] M. Krämer, J. Zunft, J. Steegborn and P.M. Zerwas, Phys. Lett. **B348** (1995) 657.
- [124] M. Krämer, Nucl. Phys. **B459** (1996) 3.
- [125] H1 Collaboration: S. Aid *et al* Proc. of Int. Europhysics Conf. on HE Physics, Brussels, 1995.
- [126] M.G. Ryskin, Z. Phys. **C57** (1993) 89.
- [127] S.J. Brodsky *et al* Phys. Rev. **D50** (1994) 3134.
- [128] M.G. Ryskin, R.G. Roberts, A.D. Martin and E.M. Levin, Durham preprint, DTP/95/96.
- [129] R.L. Jaffe, Comm. Nucl. Phys. **19** (1990) 239.
- [130] R. Mertig and W.L. van Neerven, Leiden preprint INLO-PUB-6/95 (revised);
W. Vogelsang, Rutherford Laboratory preprint RAL-TR-95-071.
- [131] M. Glück, E. Reya, M. Stratmann and W. Vogelsang, Dortmund preprint DO-TH 95-13 (1995), Phys. Rev. (in press);
R.D. Ball, S. Forte and G. Ridolfi, preprint CERN-TH/95-266;
T. Gehrmann and W.J. Stirling, Durham preprint DTP/95/82, Phys. Rev. (in press).
- [132] T. Gehrmann and W.J. Stirling, Proc. of the Workshop on the Prospects of Spin Physics at HERA, Zeuthen, August 1995, eds J. Blümlein and W.-D. Nowak (1995), p.295.
- [133] J.D. Bjorken, Phys. Rev. **148** (1966) 1467; *ibid.* **D1** (1970) 465; *ibid.* **D1** (1970) 1376.
- [134] S.A. Larin, F.V. Tkachev and J.A.M. Vermaseren, Phys. Rev. Lett. **66** (1991) 862; S.A. Larin and J.A.M. Vermaseren, Phys. Lett. **B259** (1991) 345.
- [135] A.L. Kataev and V. Starchenko, CERN-TH-7198/94.
- [136] J. Ellis and R.L. Jaffe, Phys. Rev. **D9** (1974) 1444; Erratum *ibid.* **D10** (1974) 1669.
- [137] S.A. Larin, Phys. Lett. **B334** (1994) 192.
- [138] A.L. Kataev, Phys. Rev. **D50** (1994) 5469.
- [139] C.S. Lam and Bing-An Li, Phys. Rev. **D25** (1982) 683.
- [140] R. Voss, Proc. of the Workshop on the Deep Inelastic Scattering and QCD, Paris, April 1995, eds J.-F. Laporte and Y. Sirois, p.77.
- [141] SMC: B. Adeva *et al* Phys. Lett. **B302** (1993) 533.
- [142] SMC: D. Adams *et al* Phys. Lett. **B357** (1995) 248.
- [143] SMC: D. Adams *et al* Phys. Lett. **B329** (1994) 399; erratum, Phys. Lett. **B339** (1994) 332.
- [144] SMC: B. Adeva *et al* Phys. Lett. **B336** (1994) 125.
- [145] E142 Collaboration: P.L. Anthony *et al* Phys. Rev. Lett. **71** (1993) 959.
- [146] E143 Collaboration: K. Abe *et al* Phys. Rev. Lett. **74** (1995) 346.
- [147] E143 Collaboration: K. Abe *et al* Phys. Rev. Lett. **75** (1995) 25.
- [148] E143 Collaboration: K. Abe *et al* Phys. Rev. Lett. **76** (1996) 587.
- [149] SMC: B. Adeva *et al* Phys. Lett. **B369** (1996) 93.
- [150] V.N. Gribov, V.G. Gorshkov, G.V. Frolov and L.N. Lipatov, Sov. J. Nucl. Phys. **6** (1967) 95.
- [151] J. Bartels, B.I. Ermolaev and M.G. Ryskin, DESY preprint 95/124.
- [152] R. Kirschner and L.N. Lipatov, Nucl. Phys. **B213** (1983) 122.
- [153] J. Kwieciński, Durham Preprint DTP/95/98, to appear in Acta Phys. Polon.
- [154] J. Bartels, B. I. Ermolaev and M. G. Ryskin, DESY preprint 96-25.
- [155] Proc. of the Workshop on the Prospects of Spin Physics at HERA, Zeuthen, August 1995, eds J. Blümlein and W.-D. Nowak (1995), p.76-99.
- [156] *ibid.*, p.248-282.